DEVELOPMENT OF A CELL SORTING PLATFORM BASED ON MAGNETIC LEVITATION PRINCIPLE

A Thesis Submitted to
The Graduate School of Engineering and Science of
İzmir Institute of Technology
In Partial Fulfilment of the Requirements for the Degree of
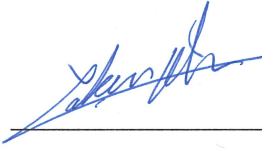
MASTER OF SCIENCE

in Biotechnology

by
Esra YILMAZ

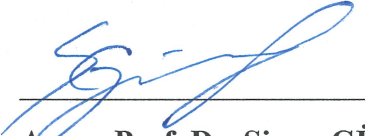July 2019
İZMİR

We approve the thesis of **Esra YILMAZ**

Examining Committee Members:

_____
Asst. Prof. Dr. Hüseyin Cumhur TEKİN
Department of Bioengineering, İzmir Institute of Technology

_____
Assoc. Prof. Dr. Özden YALÇIN-ÖZUYSAL
Department of Molecular Biology, İzmir Institute of Technology

_____
Assoc. Prof. Dr. Sinan GÜVEN
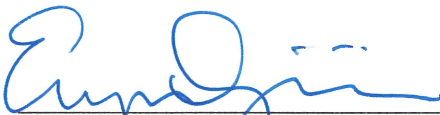Department of Medical Biology, Dokuz Eylül University

17 July 2019

_____
Asst. Prof. Dr. Hüseyin Cumhur TEKİN
Supervisor, Department of Bioengineering
İzmir Institute of Technology

_____
Assoc. Prof. Dr. Engin ÖZÇİVİCİ
Co-Supervisor, Department of
Bioengineering
İzmir Institute of Technology

_____
Assoc. Prof. Dr. Engin ÖZÇİVİCİ
Head of the Department of Biotechnology
and Bioengineering

_____
Prof. Dr. Aysun SOFUOĞLU
Dean of the Graduate School of
Engineering and Sciences

ACKNOWLEDGEMENTS

ABSTRACT

DEVELOPMENT OF A CELL SORTING PLATFORM BASED ON MAGNETIC LEVITATION PRINCIPLE

Circulating Tumor Cells (CTCs) play a vital role in cancer diagnosis, prognosis and personalized medicine. However, CTCs are extremely rare in blood (i.e., down to 1-100 CTC per 1 mL human blood) and hard to isolate because of the heterogeneity of CTCs in biomarker expression. The current CTC separation techniques use numerous differences between cells such as size, electric charges, density and expression of cell surface markers. However, these techniques have many limitations in terms of manual sample preparation steps, inconsistent results caused by low specificity and efficiency, and increased cost. Hence, there is no standard method for isolating CTCs yet. With this study, it was aimed to fill the gap in CTC isolation by proposing a new method based on magnetic levitation principle, which has recently been demonstrated as a highly acceptable method for biological characterization of cells and monitoring of their cellular events. Short while ago, magnetic levitation technology has been used to measure cell densities at single-cell level. By using this technology, unique differences in levitation height and so in density have been identified between cancer cells and blood cells. In this study, we have been developed a new label-free microfluidic cell sorter that is based on the principles of magnetic levitation. After successfully completing this master thesis, this device can be used for rapid, low cost and label-free *in-vitro* diagnosis of cancer by sorting CTCs from whole blood in a high-throughput manner. The sorted cells might further be collected for downstream analysis for personalized and precision medicine.

ÖZET

MANYETİK LEVİTASYON PRENSİBİNE DAYALI HÜCRE AYRIŞTIRMA PLATFORMU GELİŞTİRİLMESİ

Dolaşımdaki tümör hücreleri (CTC), kanser tanısında, öngörüsünde ve kişiselleştirilmiş tedavi yöntemlerinin belirlenmesinde kritik bir öneme sahiptir. Ancak, CTC'lerin kandaki sayıları çok azdır (1 mL kan içerisinde 1-100 CTC gibi), hem de biyomarker bağlamında heterojen olduklarından izole edilebilmeleri oldukça zordur. Güncel olarak kullanılan CTC ayrıştırma yöntemleri, bu işlem için hücreler arasındaki boyut, elektrik yükü, özkütle ve hücre membran antijenlerindeki farklılıkları kullanmaktadır. Ancak, söz konusu teknikler örneklerin manuel olarak hazırlanmasına, düşük ayrıştırma saflığı ve verimliliği dolayısıyla tutarsız sonuçlara ve yüksek maliyetlere neden olup sıkıntılara yol açabilmektedir. Bu nedenle, CTC'leri ayrıştırma konusunda bugüne kadar etkin ve standart bir yöntemin geliştirilemediği söylenebilir. Bu yüksek lisans tez çalışması ile CTC'lerin ayrıştırılmasına ilişkin söz konusu boşluğun son dönemde hücrelerin ve hücresel etkinliklerin biyolojik karakterizasyonu ve gözlemlenmesi konularında oldukça başarılı bir metot olarak ortaya sunulan manyetik levitasyon prensibine dayalı yeni bir yöntem geliştirilerek doldurulması hedeflenmektedir. Manyetik levitasyon teknolojisi ile, levitasyon yüksekliği ve özkütlelerdeki özgün farklılıkların belirlenebilmesi, kanser hücrelerinin kan hücrelerinden ayırt edilebilmesine imkan vermektedir. Sunulan tez çalışmasında, manyetik levitasyon prensibine dayalı, yeni ve işaretleme yöntemi kullanılmaksızın bir mikroakışkan hücre ayıracının geliştirmesi hedeflenmiştir. Mikroakışkan kanalı çevreleyen ve sabitlenen iki mıknatıs yardımıyla meme kanseri hücrelerinin sürekli bir akış halinde olan akyuvarlar arasından ayrıştırılmasını sağlayacak bir mikroakışkan cihaz tasarlanıp geliştirilmiştir. Tez çalışmasının başarıyla sonuçlanması ile çıktı olarak elde edilen bu mikroakışkan cihaz, CTC'lerin kandan büyük hacimlerde ve verimli bir şekilde ayıklanabilmesini sağlayarak kanserin hızlı, ucuz ve işaretleme yöntemlerinden bağımsız in-vitro tanısı amacıyla kullanılabilecektir. Bununla birlikte bu yöntemle ayıklanan hücreler, ileride kişiselleştirilmiş tedavi yöntemleri ve hassas tıp alanlarında kullanılmak üzere toplanıp analiz edilebileceklerdir.

TABLE OF CONTENT

LIST OF FIGURES

CHAPTER 1

INTRODUCTION

Cell sorting is generally used for enrichment and purification of cells from complex and heterogeneous mixtures into well-defined populations based on a distinct signature of interest to increase efficiency in the life sciences and in medicine [1-3].

The requirement to sort cells is rapidly growing toward the isolation of rare cell populations for cancer diagnostics, cell therapeutics and stem cell research, including the enrichment of circulating tumor cells (CTCs), hematopoietic stem cells (HSCs) and circulating fetal cells (CFCs) from blood [2, 4].

Cancer metastasis is the major cause of cancer- related death [5]. Feasible tumor cells frequently change their genetic and biological forms to manageability to invade blood vessels and migrate around the body as circulating tumor cells (CTCs). It has been verified that the number of CTCs present in a cancer patient powerfully correlates with prognosis, accomplish to predicting disease progress and effectiveness of treatments. Hence, there is a great challenge in the detection and capture of CTCs because of the number of CTCs in the peripheral blood range from one (if at all possible) CTC per 10 ml capable to hundreds of CTCs per ml [5-9] even biomarkers on the surface of the CTCs or inside the cells are not abundant. [10].

The separation/sorting techniques were classified by the induced cell properties by fluorescent and magnetic labels, size, shape, density, compressibility, deformability, cell surface markers, dielectric and intrinsic magnetic properties to distinguish cells.

1.1. Conventional Cell Sorting Methods

Conventional cell sorting methods based on flow cytometry and relies on fluorescent probes, stains and magnetic tags to classify cells by type.

1.1.1. Fluorescence-Activated Cell Sorting

In 1969, Herzenberg et al. introduced the first commercial cell sorter, which uses a technique chiefly known as fluorescence-activated cell sorting (FACS) [11-13]. Fluorescence Activated Cell Sorting (FACS), is one the most complex and customer friendly technique for characterizing and defining different cell types in a heterogeneous cell mixture based morphological and fluorescent cell signatures (cell surface, cell size and granularity) [14, 15].

FACS technology enable sorting or quantitative and qualitative analyses of heterogeneous or single cells into different vessels [14-16]. Before separation, the target cells are labeled with a fluorescent probe contingent on cytometry facilities and on experimental apparatus. For example, if the sorter apparatus has three lasers, capable to twelve different parametric quantity which consist of cell viability, apoptosis, necrosis, membrane potential and cell cycle stage etc. [12, 15]. The frequently used lasers are the 488 nm (>20 mW) and 633 nm (>18 mW). However, depending on the tests various extra laser can be preferred containing 375 nm (>7 mW), 405 nm (>50 mW) and 561 nm (>18 mW) [15].

Fluorophore conjugated monoclonal antibodies are extensively used fluorescent probes (mAb) that identifies explicit cell surface markers on target. FAC sorter separates target cells according to selected characteristics via two stage protocol. Firstly, the optical detection system identifies the presence of fluorescent markers (that have been tagged to targeted ones only) in a stream of cell suspension. As a single cell pass through the cytometry, the detector measures light scatter from the emitting fluorophores. Whenever a cell of interest is identified, the charged cell is electrostatically deflected to separated collection tubes by an electric deflection system for later assays (Figure 1.1.) [14, 15, 17]. On the bleeding edge, FACS can sort particles or cells up to 50 000-100 000 particles/cells per second and are competent to identify 14-17 varied fluorescent markers [17-19].

Nevertheless, FACS has been widely utilized in clinical diagnostics, it has several limitations. First, FACS needs a large starting number of cells. Hence, this method cannot succeed to sort single cells from a low quantity cell mixture. Secondly, in this approach stimulation experiments of cells and cell cultures are essential and they must to treated in a separate surrounding before FACS analysis [2, 14, 17, 20].
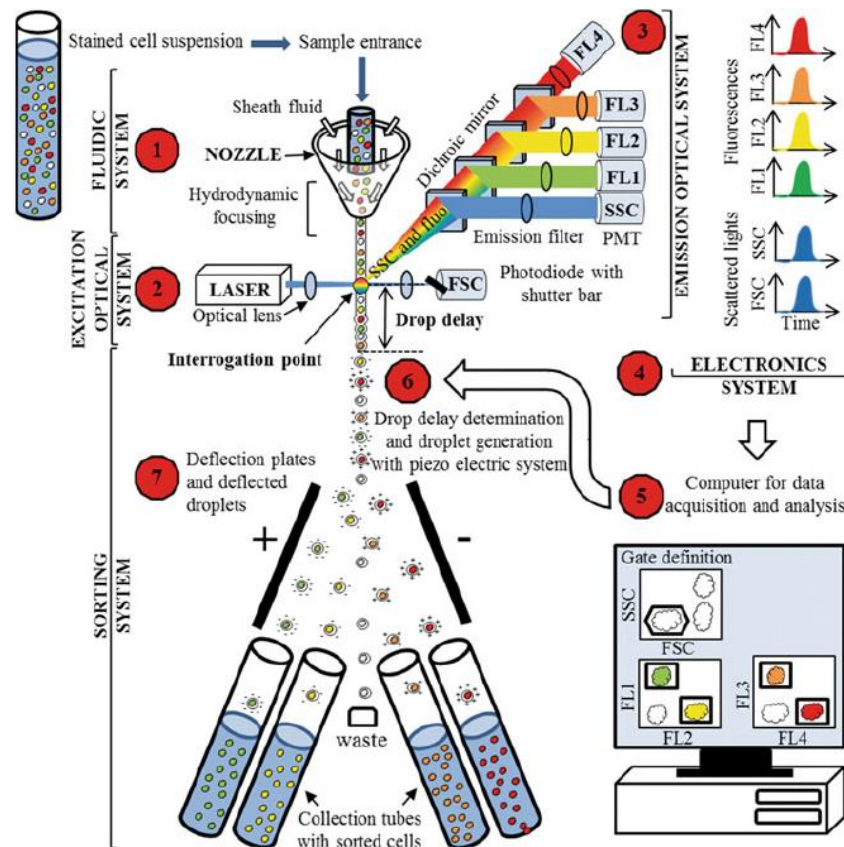
Figure 1.1. Schematic of Fluorescence Activated Cell Sorting (FACS)
(Source : Hu et al., 2016 [14] ; Picot et al., 2012 [20])

The loss of viability in sorted cells can be explained by high-speed flow in the sorter and non-specific fluorescent molecules. Moreover, these systems need high investment of capital [2, 14, 17, 20].

1.1.2. Magnetic-Activated Cell Sorting (MACS)

Magnetic-activated cell sorting (MACS) is the other widely used antibody labeled approach an alternative to FACS. In this method, before sorting target cells are tagged with marker specific antibodies coupled-magnetic labels. When a mixture of heterogeneous cell population containing tagged and untagged cells flowed through an external magnetic field, the magnetically tagged cells are leaded to the collection tubes by strong magnetic force (Figure 1.2) The unlabeled cells can be gathered by washing steps after the magnetic field is turned off.

3
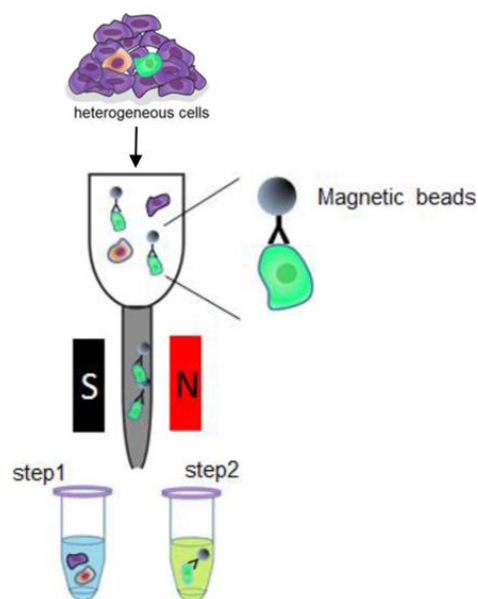
Figure 1.2. Schematic of Magnetic Activated Cell Sorting (MACS)
(Source: Hu et al.,2016 [14])

Unfortunately, MACS can just utilize surface molecules of cells as markers for the sorting of live cells. The operation is performed in batch mode and extension of process time increases the risk of the cross contamination by non-specific binding with the magnetic tags. Moreover, MACS is much more limited than FACS due to using immunomagnetic techniques that can simply split cells into positive and negative populations. Using high and low expression level of a molecule, it is not possible to separate whereas it is workable by the way of FACS. Although, MACS technology is simple and provides cost effective sorting compared to FACS, many commercial kits are available on the market. The US Food and Drug Administration (FDA) approved CELLSEARCH® system allows isolation of circulating tumor cells (CTCs) from a 7.5 mL blood sample based on the identification of the epithelial cell adhesion molecule (EpCAM). This commercial sorter is useful for bulky CTC populations but cannot be integrated exactly with well plates for molecular analysis of single cells [2, 4, 14, 17, 19, 21, 22].

These two separation techniques have been mostly used as modern tools in basic and clinical applications. However, to eliminate their drawbacks microfluidics-based cell sorting systems become an alternative and powerful mechanisms that provide cost effective, high purity and high throughput isolation and succeeding analysis of various cell types.

1.1.3. Density Based Sorting

Ficoll density gradient separation was used to enrich peripheral blood mononuclear cells (PBMCs), contain CTCs from whole blood [23-28] in CTC Scope™ (ACD) system for sample preparation of PBMCs and the pre-enrichment of CTCs in the EPithelial ImmunoSPOT (EPISPOT,CHU, Montpellier & UKE, Hamburg) assay which is a method for detecting proteins secreted from CTCs [29]. However, density gradient mediums, such as Ficoll and Hypaque have toxic effects on CTCs in prolonged exposure time [29]. In a study, the effectivity of Ficoll density gradient separation was investigated and resulted in a 24 % recovery rate [30].

Cell density changes are closely related to cell state and differentiation [31, 32]. Cell densities can be measured by using different technologies including density-gradient centrifugation, suspended microchannel resonator (SMR) [33] and optically induced electrokinetics (OEK) [34]. However, these approaches either allow the density measurement of bulk cell populations (not possible to detect the density changes at single cell level with current methodologies) or their applications are quite limited because of the expensive and complex operation prerequisites [31, 32].

1.2. Microfluidic Cell Sorting Methods

Over the past 30 years, the first analytical miniaturized device fabricated on silicon, a gas chromatographic analyzer, was introduced. This notable gas chromatography device was capable of separation of a simple solution of compounds in a matter of seconds [35].

In the late 20th century, attention in the conception of micro total analysis system (µTAS) or lab-on-a-chip (LOC) systems have grown explosively. Various analytical processes were miniaturized into the small scale and integrated with other analysis systems. The development in this system proffers a novel perspective over earlier laboratory protocols. The power to conduct laboratory procedures on micro-, nano- or pico-scale, using miniaturized devices have offered a new approach in modern analytical

chemistry, medicine, genetic, cell biology and many other research disciplines. Microfluidic lab-on-a-chip (LOC) devices have proven to be a promising platform instead of conventional applications due to a number of benefits such as small size, low-cost, low sample and reagent consumption, portability and besides fast analysis time [35-41].

1.2.1. Sorting Based on Size, Shape and Deformability

Cell separation by physical properties such as size, shape, and deformability attract a great deal of attention for real time medical diagnosis and biological applications. This label-free approach does not need expensive reactive agents or antibody labeling thus and so decreasing sample preparation time while enhancing throughput and cell viability. Commercially available CTC separation system, Parsortix (ANGLE, UK) utilized size based filtration for rare cells from blood and succeed in capture efficiency of 66 % [42]. Fan et al. achieved > 90 % recovery by the time isolation of lung cancer cells from a spiked blood sample with comparatively high processing throughput of 10 mL/h [17, 43]. Tang et al. developed conical micro holes filters that enable the capture of CTCs of 96% purity under 0.2 mL/min flow by designing the two-level microfluidic device using biocompatible materials (Figure 1.3.a). Furthermore, the designed microfluidic device makes possible to culture captured CTCs [44].

Microfluidic devices using inertial forces within the fluid flow to separate differently sized particles/cells along the microfluidic channel due to the force balance between the inertial lift force and the Dean drag force. The fluid flow contains cells that must be high enough to create adequate deflection. Such inertial based methods have been proved for separating, offers a wide range of flow rate from 5 µL/minute to 8 mL/minute. Therefore, these devices using inertial focusing are efficient approaches to succeed a continuous, fast, and high throughput sorting of tumor cells.

Papautsky and co-workers improved a two-phase separation method for blood and tumor cells [45]. The first part of the design takes advantage of inertial lift force to direct cells into two flow. Flows from the initial part pass the second part where rotational lift forces filter cells in company with improved efficiency. The thrived sorting efficiency of Human Prostate Epithelial (HPET) tumor cell is 99 % from diluted blood [45, 46].
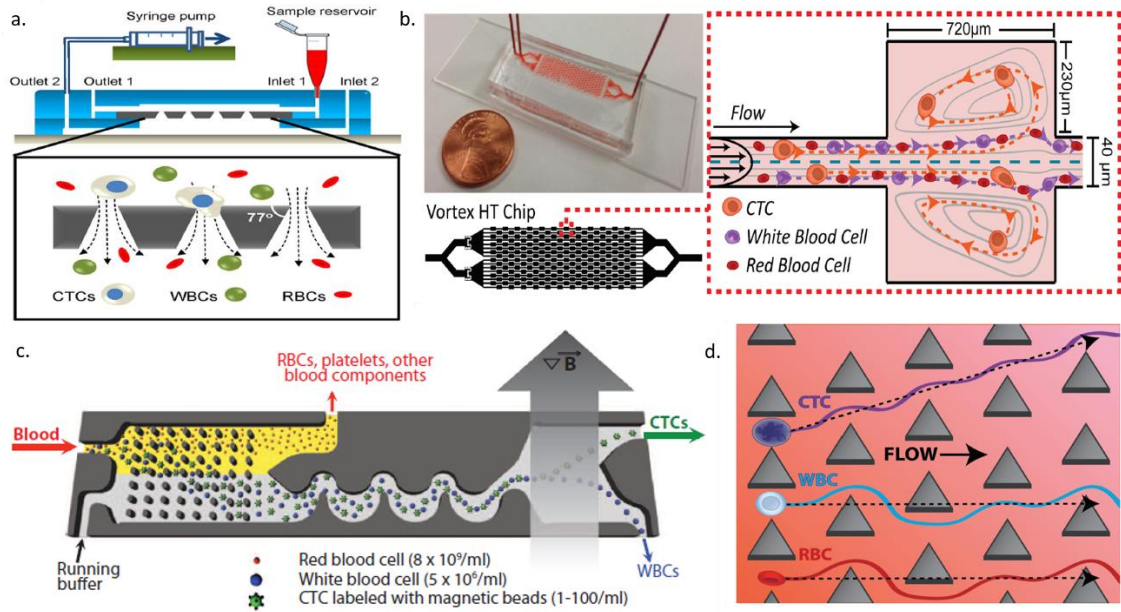
Figure 1.3. Separation Based on Size, Shape and Deformability. a) Conical Membrane Filter (Source: Tang et al., 2014 [44]), b) High Throughput Vortex Chip (Vortex HT) (Source: Che at al., 2016 [47]), c) CTC-iChip (Source: Ozkumur et al., 2017 [48]) and d) Deterministic Lateral Displacement (DLD) Array (Source: Loutherback et al., 2012 [49]).

Che at al. demonstrated a high throughput vortex chip (Vortex HT) includes the additional two parallel channels and reservoirs in series to their previous study to enhance capture efficiency of CTCs up to 83 % [47]. The developed Vortex HT proceeds 8 mL of 10x diluted blood in min to separate MCF-7 cells with an 85% purity (Figure 1.3.b) [47, 50].

Abdulla et al. designed cascaded microfluidic channels to isolate two different types of CTCs from blood cells using inertial focusing [51]. Human lung cancer cells (A549) and human breast cancer cells (MCF-7) were precisely sorted out human blood [51]. In addition, the viability of these two tumor cells were more than 95 % after separation process [51]. CTC-iChip combination of hydrodynamic, inertial focusing and magnetophoresis approaches was introduced to sort CTCs from whole blood at 10^7 cells/second throughput by Ozkumur et al. (Figure 1.3.c) [48].

In the deterministic lateral displacement (DLD) technique, cell populations can be separated predicate on differences the set of properties includes size, shape and deformability. The fluid flow through an array of microstructures and are differentially moved when the flow forces particles/cells surrounding microstructures obstacles. In this system, particles/cells smaller than critical hydrodynamic radius direct with the convective flow whereas particles/cells with a larger radius than crucial radius collide

with posts and are demonstrated lateral displacement oppose the direction of smaller ones. Consequently, differently sized particles/cells can be concentrated in outlets differently [17, 52-54]. Liu et al observed the separation of MCF-7 and MBA-MB-231 tumor cells from blood and the isolation efficiency of their device are 99 % for MCF-7 and 80 % for MDA-MB-231 at a throughput of 2 mL/min [55]. Using a triangular pillar shown in Figure 1.3.d, Loutherback et al. isolated CTCs with a capture efficiency of 85 % from blood without affecting cell viability at a throughput of 10 mL/min [49].

1.2.2. Sorting Based on Size, Density and Compressibility

1.2.2.1. Centrifugation and Pinched Flow Fractionation (Size and Density)

Density gradient centrifugation is a conventionally used technique to separate particles within the bulk. In this method, centrifugal force is used to separate cells that rely on the sedimentation coefficient differences of cells. The sedimentation rate of a cell within a fluid with a mixture of densities depends on the size and the density of the cell and correlates with the density of the fluid. When a fluid is exposed to centrifugal force, the particles with different densities move through the density gradient at unique rates depending on their density and create density bands that can be seen obviously. The denser cell, RBC (density: ~ 1.1 g/mL), becomes visible at the bottom of the tube while the CTC (density of <1.077 g/mL) rests at the top of the solution [56].

Lee et al. developed a centrifugal force and size selective based CTC-isolation device, described in Figure 1.4.a, that can separate CTCs from whole blood in 30 seconds with high purity [57]. The platform was achieved a capture efficiency of 61 % of MCF-7 within whole blood by favor of the integration of size based filtration system [57].

Using pinched flow fractionation (PFF), cells are brought into focus inside a narrow channel and suddenly spiked an extended area and come under the effect of gravitational, drag and buoyancy forces. Cells that are less dense than the surrounding medium will be lifted to the upper regions of the expanded chamber.
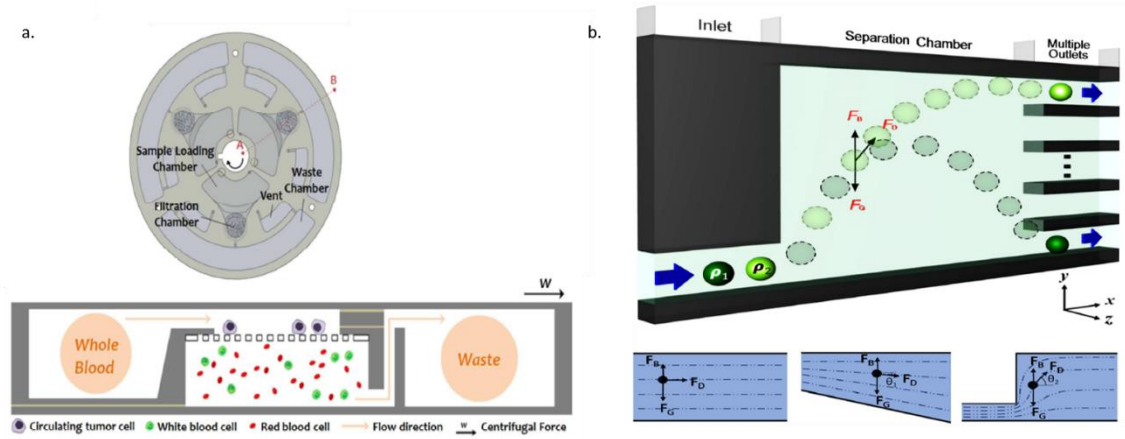
Figure 1.4. Size and density-based separation devices. a. The top and cross-section view of the CTC isolation platform includes loading chamber, filtration chamber, waste chamber (Source: Lee at al., 2014 [57]) and b. The illustration of density difference amplification-based cell sorting (dDACS) device, which comprise an inlet, a separation chamber and multiple outlets and feasible microfluidic channel configurations; uniform channel height (left), gradual channel expansion (middle), and hydraulic jump cavity with sudden channel expansion (right) (Source: Song et al., 2014 [58]).

Cells with higher density will experience greater gravity force and flow towards the bottom of the chamber. Song et al. demonstrated label-free density difference amplification-based cell sorting (dDACS) device which achieve the separation of particles by getting different heights at the outlet chamber due to the their density, depicted in Figure 1.4.b [58]. Particles in different densities ($q_1 > q_2$) go through the separation chamber and gravitational (F_g), buoyancy (F_b), and drag (F_d) forces effects on them along the channel. In the separation chamber due to density difference of the particles, they reach separation heights distinctly and this significant difference utilize collecting particles from disparate outlets. In addition, to interfere with the height difference between particles, it is possible to broaden channel expansion/width compared to the other two cases due to the relatively large tangential angle, h of F_D $Q_1 < Q_2$ [58].

1.2.2.2. Acoustophoresis (Density and Compressibility)

Acoustic resonance inside a microfluidic channel, generated by piezoelectric substance can produce radiation forces to manipulate particles and cell populations as

label free and rapid sorting without affecting the viability [17, 53, 59]. In acoustic microfluidic platforms, high intensity sound waves interact with the channel to generate pressure gradients that move cells into specific locations and cells can be channel out from the defined locations. The acoustic waves reflected off from the microchannel walls establish a standing wave pattern within the microchannel. Cells flowing through the standing wave are moved towards high pressure or anti-pressure node by radiation forces. The magnitude of the radiation force links with the volume, density and compressibility of the cell, the surrounding medium and the amplitude and wavelength of the acoustic wave. Cells that have greater density and compressibility than the surrounding fluid travel to the pressure node. Bands of cells, grouped by density and compressibility, form across the microchannel. Since the flow is laminar, cells will hold the position in the band even after crossing the acoustic zone and conveniently collected at separate outlets.

Magnusson et al reveal a clinical scale label free the acoustic microfluidic platform, depicted in figure 1.5.a, to enrich CTCs from 5 mL of RBC depleted blood (diluted 2x) within 2 hours [60].
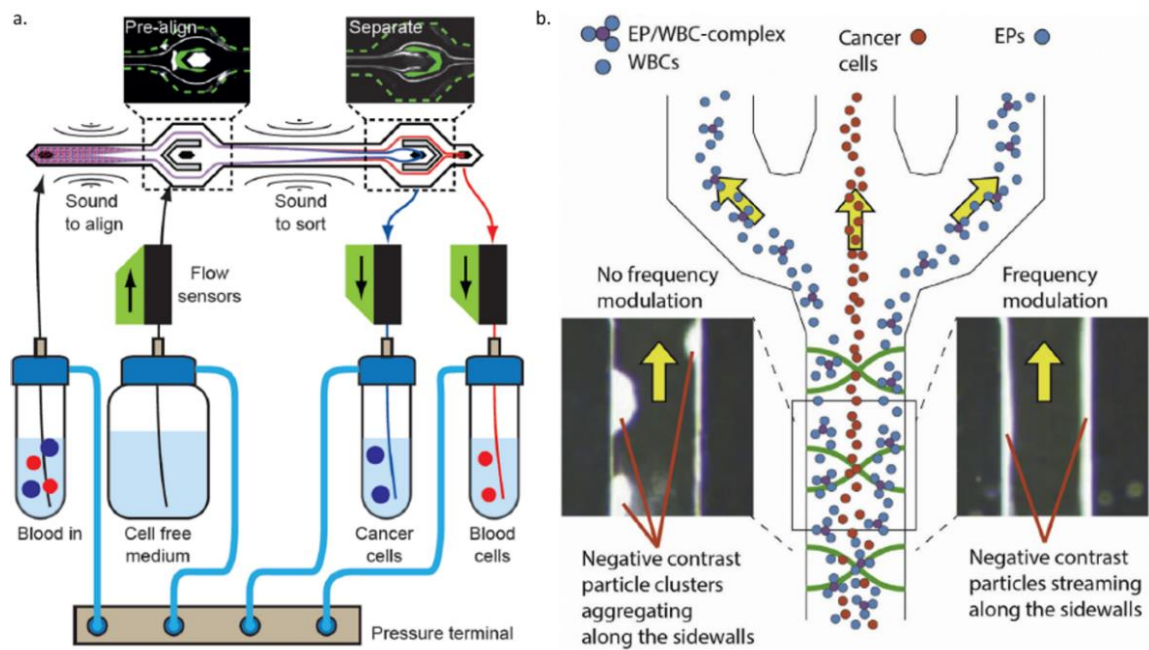
Figure 1.5. Acoustophoretic Separation. Schematic view of a) the clinical scale acoustophoretic microchip (Source: Magnusson et al., 2017 [60]) and b) the negative acoustic contrast particle immuno-acoustophoresis (Source: Cushing et al., 2018 [61]).

In this device, the sample tubes are separately pressurized and then cell solution from the sample reservoir passes into the chip through the pre-align channel. After running through the separation channel, the cells are directed in separated tubes. The reported recovery rate for MCF-7 breast cancer cell line is 86 ± 2.3% with a 75 μL/min flow rate [60].

For the first time, acoustophoretic negative selection of WBCs from cancer cells using elastomeric particles (EPs) that activated with CD-45 antibodies specific to WBCs presented by Cushing et al. and the separation efficiencies were recorded as 98.6% MCF-7 breast cancer cells and 99.7% DU 145 prostate cancer cells [61]. In figure 1.5.b, negative contrast clusters aggregate along the sidewalls without ultrasonic acoustic waves whereas negative contrast particles pass through microchannel under actuation frequency [61].

1.2.3.   Sorting Based on Dielectric Properties

Dielectrophoresis (DEP), a label-free separation method based on the differences of the dielectrical characteristics of cells is operated with a force is induced on a dielectric particle when it is in a non-uniform electric field. DEP was widely studied for the sorting of rare cells, blood cells, yeast and bacterial cell [2, 62]. Because most of the biological cells have dielectric properties in an external electric field, cells in suspension can be controlled by a DEP force. The cells can be stimulated to attract towards the region of a maximum electric field by a positive DEP force or on the other hand, to deflect the area with a weak electric field by a negative DEP force in the non-uniform electric field. The general working strategy of DEP is to lead the deflections of target cells to separate them from a flow. By using a DEP technique, a high recovery rate and purity can be achieved with an optimum flow rate, where the DEP strategy acting on a target cell is larger than the fluidic drag force. The dominant DEP force allows the cell sample to move towards or away from the electrodes, rather than following the sample flow [2, 17, 53, 54].

The integration utilizes the increasing of the performance of DEP devices by attaining a pre-separation step before the DEP practices. In multi-orifice flow fractionation (MOFF) part of the integrated system, cells are moved laterally supply the concentration of cells at distinct positions inside the channel because of the hydrodynamic

forces [63]. At the first separation part, larger MCF-7 cells and a few blood cells move into the middle channel and participate in the DEP channel, after which most blood cells collected from outlet I. In the focusing region, all cells are influenced a positive DEP force and so align along both sides of the channel. Lastly, in the second region, MCF-7 cells were isolated by DEP forces which enhance the efficiency of the sorting. After the serial combination of the mentioned separation procedure, 75.81 % of MCF-7 cells were isolated from outlet II while 99.24% of RBCs and 94.23% of WBCs were removed at a 126 µL/min flow rate, depicted in Figure 1.6.a [63].
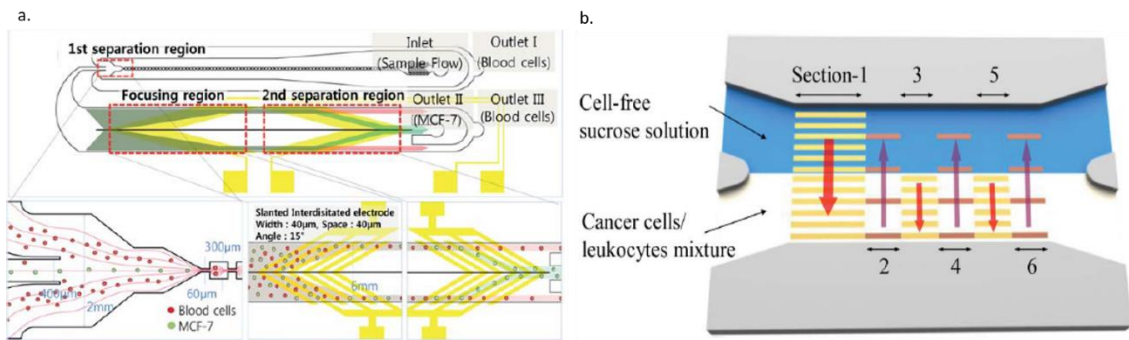
Figure 1.6. Sorting based on dielectric properties. a) Schematic illustration of multi-orifice flow fractionation MOFF integrated DEP microfluidic device (Source: Moon et al., 2011 [63]) and b) the top view of dielectrophoretic (ODEP) force-based cancer cell separation device includes six zones (Source: Hung et al., 2013 [64]).

To isolate circulating tumor cells (CTCs) negatively, the set of optically induced dielectrophoretic (ODEP) force-based cell manipulation and the laminar flow in a microfluidic system were presented by Huang et al.[64]. In the figure 1.6.b, cell-free sucrose solution and cancer cells/leukocytes mixture were loaded and then six sections of moving light-bar screens were continuously and concurrently exerted at the CTC isolation zone. The operational protocol of the ODEP force-based device to exert CTCs from blood background effectively is primarily due to the differences in the size of CTCs and electrical properties. Using optically induced dielectrophoretic force, prostate cancer (PC-3) and human oral cancer (OEC-M1) cells were exerted from with recovery rates 76–83 % and 61–68 % respectively and at a 0.1 µL/min flow rate [64].

1.2.4. Sorting Based on Intrinsic Magnetic Properties of Cells

As another method, separation can be achieved by gaining an advantage from the intrinsic magnetic properties of red and white blood cells. Deoxygenated RBC, the most paramagnetic cell in the body, is naturally paramagnetic which means this cell is directed towards to magnetic field. On the other hand, since oxygenated RBCs and WBCs are diamagnetic, they deflect from the magnetic field [37, 65-67].

Furlani introduces a device that provides directly and continuously isolation of RBCs and WBCs from plasma by engrafting a microarray of soft magnetic elements [65]. When they were magnetized, deoxygenated RBCs were attracted and WBCs were deflected into two outlets and plasma expelled from the middle outlet. Using a similar approach, RBCs from whole blood were isolated. When the blood sample was treated with $NaNO_2$, the hemoglobin in the RBCs was changed form to paramagnetic. They attained 93.5% efficiency using diluted blood (1:40) at a flow rate between 0.12 to 0.92 µl/min under a magnetic field (0.2 T) [65]. Nam et al present a study that considers malaria infected RBCs since malaria by-product, hemozoin, give magnetic property to red blood cells [67]. Firstly, they fabricated PDMS channel that has integration with a wire bonded on a glass surface. Then, the device was used to separate with a recovery rate of 73% and 98.3% for early-stage i-RBCs and late-stage i-RBC, respectively [67].

Using the magnetic susceptibility differences between cells and gadolinium diethylenetriamine Penta acetic acid (Gd−DTPA) which is a biocompatible paramagnetic salt solution, U-937 cells from RBCs were separated via magnetophoresis without the use of any label [68]. Using permanent magnets, nickel (Ni) structures have been engrafted into the system, magnetic field was created to the (PDMS) channel without the use of high Gd−DTPA concentrations. The microfabricated design supplies a strong magnetic field from permanent magnets. The value of the magnetic repulsive force differences acting on cells in different sizes are increased by calibrating the magnetic susceptibility of the surrounding medium, which depends on the concentration of (Gd−DTPA). To prove the label-free concept, two differently sized polystyrene (PS) beads, 8 and 10 µm in diameter, were preferred to evaluate separation efficiency. By courtesy of increment of the Gd−DTPA concentration from 0 to 40 mM, the separation resolution of polystyrene beads was increased from 0.08 to 0.91. Moreover, the separation of U-937 cells from RBCs was

succeeded with >90 % purity and 10^5 cells/h throughput at 40 mM Gd based solution (F. Shen, Hwang, Hahn, & Park, 2012).

1.2.5. Sorting Based on Cell Surface Markers Properties

Separation or enumeration by cancer cell surface marker features were conventionally applied to isolate CTCs from whole blood. Target CTCs are selectively captured on surfaces functionalized with epithelial cell adhesion molecule (anti-EpCAM) antibodies under laminar flow considerations. Adversely, the detection of CTCs by using surface markers are limited because of the 'stealthy' action during epithelial mesenchymal transitions (EMT) when the surface markers are absent or reduced, still challenging to improve the capture efficiency of CTCs [2, 17, 69, 70].

To increase the capture efficiency of MCF-7 cells, Gaskill et al. immobilized E-selectin which is an adhesion molecule to the surface of the channel by providing the bonding of leukocytes to E-selectin [17]. By force of bonding, leukocytes come together close to the capture surface and obstruct flow to enlarge CTC contact area with anti-EpCAM on the surface and via this modification capture efficiency reached to 98 % at a flow rate of 18.7 µL/min [17]. The spiral shape channel was designed to capture both MCF-7 and MDA-MB-231 cells that are originated from breast carcinoma cell by Kwak research group [71]. The simply designed system revealed the separation of these cancer cells as well as identified cancer cells according to their EpCAM expression level. Using magnetic nanoparticles, EpCAM positive and negative cells were captured with 96.3 % and 81.2 % efficiency at a flow rate of 150 µL/min [71].

In particle based magnetic cell sorting, cells of interest are incubated with marker specific antibodies conjugated to magnetic particles contain iron that provides the recognition under the influence of magnetic forces. When a magnetic field is applied, magnetic particles are selectively isolated or sorted from different outlets of the sorting system and thus it is immunomagnetic technique [2, 54, 62]. For positive CTC separation epithelial specific surface markers include EpCAM, EGFR, HER2 and MUC and for negative CTC separation by using leukocyte specific surface markers like CD45 and CD66b have been widely applied to obtain enriched CTCs [29]. Magnetic force gradient

based microfluidic chip (Mag-Gradient Chip) has been revealed for the isolation of CTCs and all the characterization of the status of CTCs real time in as far as the expression level of EpCAM. 95.7 % of EpCAM positive and 79.3 % of EpCAM negative CTCs were successfully isolated using the Mag- Gradient Chip with a 3 mL/h flow rate [72].

Recently, the integration of the deterministic lateral displacement (DLD) microfluidic structures with magnetic-activated cell sorting (MACS) has been presented as a novel methodology to capture tumor cells independent from their surface antigens. In the DLD part of the microfluidic structure, RBCs and platelets were removed by sized based deflection and then MACS separator helps to primarily separate unlabeled CTCs from WBCs labeled with microbeads resulted in 85 % yield of CTCs under 60 µL/min [73].

1.2.6. Sorting Based on Magnetic Susceptibility and Density

Magnetic levitation is a novel label-free technology to measure single cell density and separate microparticles and cells via negative magnetophoresis (diamagnetophoresis) based on their unique densities [31, 74, 75].

Paramagnetic salt solutions and ferrofluids were frequently used to position objects on the basis of measurement of densities in non-flow systems. This type of separation is generally called as magnetic levitation, or briefly "MagLev" [76]. Gadolinium (Gd^{3+}) based nonionic paramagnetic medium was used to detection density changes at a single cell level without the need for any biomarker. This levitation platform, MagDense, is presented as an only platform that is sensitive small differences in density of cells at higher resolution 1×10^{-4} g/mL and allow them to monitor as real-time during the label-free assay [4, 74].

The magnetic levitation platform comprises two permanent high-grade (N52) neodymium (NdFeB) magnets (50 mm length, 2 mm width and 5 mm height) with like poles facing each other and a capillary channel (1 mm × 1 mm cross-section, 50-mm length) filled with Gadolinium-based solution and two tilted (45°) mirrors for observation via a microscope. Though negative magnetophoresis, diamagnetic objects /microparticles /cells tend to migrate towards larger magnetic induction site to lower site and stay at a position where the magnetic force (F_{mag}) is opposed to buoyant force (F_b) based on the

unique densities of objects (Figure 1.8.a) [74]. The levitation height of an object can be evaluated via magnetic induction (B) [37] and can be expressed as follows;

$$\frac{x_m}{\mu_0}(B.\nabla).B - \Delta\rho g = 0 \tag{1.1}$$

where g is the gravitational acceleration and μ_0 is the permeability of the free space, Δx is the magnetic susceptibility difference between the object and the surrounding magnetic solution, $\Delta\rho$ is a difference in density between the paramagnetic medium (ρ_{medium}) and cell (ρ_{cell}). When compared, the magnetic susceptibilities of cells can be ignored against the magnetic susceptibility of the paramagnetic environment. Therefore, the equilibration height of a cell is primary rely on the density of the cell.

Polyethylene density beads were used to corroborate the magnetic levitation platform before using cells. Polyethylene beads were given into the capillary channel in fetal bovine serum (FBS) contains 30 mM Gd were introduced. Density beads reached their levitation heights in a short period of time with respect to their unique densities (Figure 1.7.a). The equilibrium height of beads can be varied using different Gd concentrations (10 mM, 30 mM, and 50 mM) (Fig. 1.7.b).
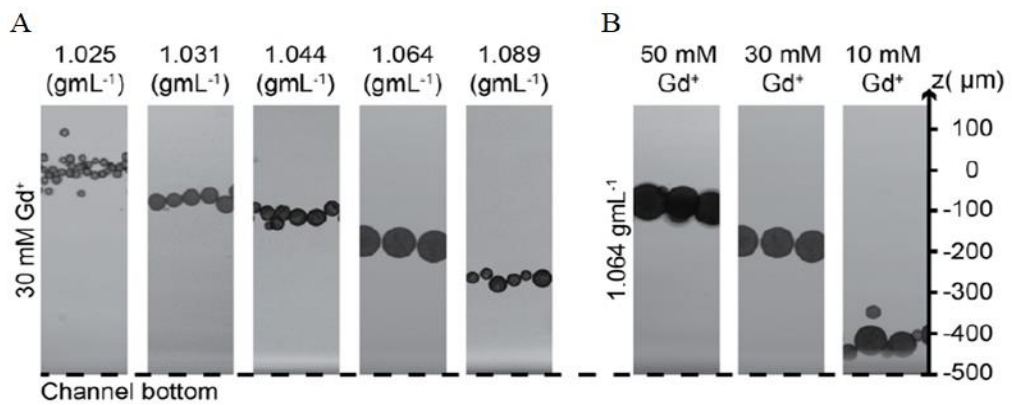
Figure 1.7. Density measurement of polyethylene density beads in the MagDense. a. Beads (diameters 10 to100 μm) with various densities (1.025 g/mL , 1.031 g/mL, 1.044 g/mL, 1.064 g/mL, and 1.089 g/mL) and their characteristic levitation heights in 30 mM Gd. b. 1.064 g/mL density beads had distinct levitation heights in different Gd concentrations (10 mM, 30 mM and 50 mM) (Source: Durmus et al., 2015 [74]).

To evaluate the capability of the MagDense platform with respect to characterization of cells, different mammalian cell line including breast adenocarcinoma (MDA-MB-231), esophageal adenocarcinoma (JHEsoAD1), colorectal adenocarcinoma (HT29), colorectal carcinoma (HCT116), nonsmall cell lung adenocarcinoma (HCC827) and blood cells (WBC and RBC) were levitated in a capillary channel containing 30 mM Gd solution in FBS and measured densities (Figure 1.8). In a short period of time, these cells were equilibrated at unique levitation heights, forming distinct density bands specific to cells (Figure 1.8.b). The distinctive levitation heights of the all types of tumor cells and blood cells were closely linked with their density and magnetic susceptibilities.
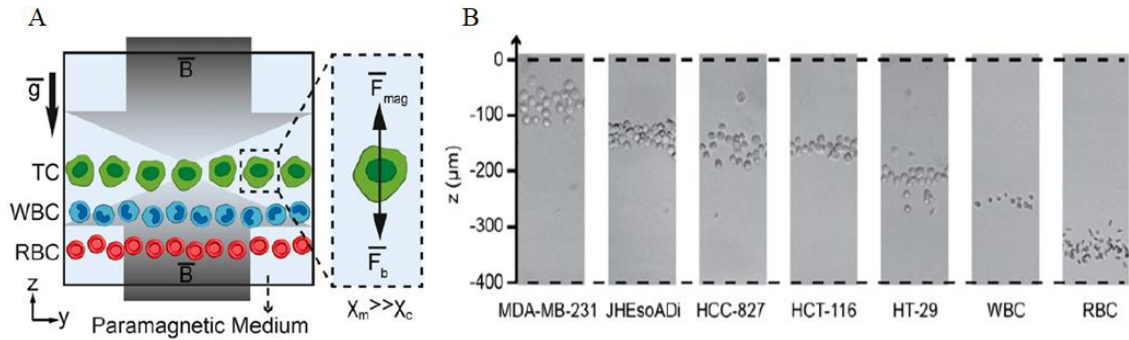
Figure 1.8. Density-based microfluidic cell separation device. a) The working mechanism of MagDense and b) Levitation heights of several types of tumor cells and blood cells along the channel (z-axis) in the MagDense (Source: Durmus et al.,2015 [74]).

As an alternative, to get rid of the adverse effect of the cell labeling, ferrofluids (e.g. water containing iron-oxide Fe_2O_3 nanoparticles) have been used to enhance the magnetic repulsive force by raising magnetic susceptibility of the surrounding medium [4,68]. When non-magnetic microparticles are mixed with ferrofluids and then are loaded into the microfluidic channel, non-magnetic particles deflect from their flow patterns since the magnetic buoyancy forces act on them under non uniform magnetic field [77]. Larger particles are under the influence of magnetic forces, directly proportional to the volume of the non-magnetic particles, more than smaller particles. Additively, the hydrodynamic drag force is estimated with the diameter of the particles. Consequently, particles of larger size are more deflected than smaller ones [77].

Biocompatible ferrofluids have been used to separate Hela cells and blood cells with a higher recovery rate (more than 99 %) and $1x10^6$ cells/h throughput [78] additively

Ferrohydrodynamic cell separation (FCS) device have been ensured the separation of low concentration (∼100 cells/mL) cancer cells including six cancer cell line from WBCs inside biocompatible ferrofluids with an average 92.9 % cancer cell recovery rate and an average 11.7 % purity of cancer cells at a high throughput of 6 mL/h [79]. Moreover, when the cancer cell concentration has been downed to ∼10 cancer cells/mL, almost 99 % recovery rate has been achieved as a result of 12 mL/h throughput [80]. However, due the opaque property of ferrofluids, their usage in cell sorting methods are restricted as it is impossible to observe if a fluorescent dye is not used. Paramagnetic salt solutions are more favorable than ferrofluids because of their transparent property [68].

Congruently to the presented previous study by Durmus et al, using magnetic levitation principle, characterization of densities of MDA-MB-231 breast cancer and A549 lung cancer cells where that were embedded into gels at different collagen concentrations was achieved [81]. The results show that density values of MDA-MB-231 cells extracted from the collagen gels were more dramatically spread widen whereas no significant density differences of the A549 cell lines were observed. These experiments were proved that the density platform can be used for the monitoring of cancer cells in density measured device help to get more information about changes of phenotypic properties of cells which related to extracellular matrix stiffness [81].

The aim of this study is instead of complicated and expensive devices that require specially trained personnel for the use of cancer cells to distinguish them from blood cells, it was ensured to design and develop a platform which is independent of the labelling technique, single-use and therefore cheap through the use of magnetic levitation principles. The proposed technology will allow the diagnosis of cancer by sorting CTCs from whole blood. In addition, isolated CTCs with this novel technology can be used in transcriptomic and proteomic analyzes sensitively in personalized medicine. Thus, the technology to be developed with this master thesis will find a wide range of applications in the medical field.

CHAPTER 2

MATERIALS & METHODS

2.1. Materials

2.1.1. Consumables and Chemicals

PGMEA (Propylene glycol monomethyl ether acetate, Sigma Aldrich, U.S.A.), SU-8 50 Negative Photoresist (MicroChem) and silicon wafers (Nanografi Co. Ltd.) were purchased for microfabrication. N52 grade neodymium magnets (NdFeB) (Supermagnete,U.S.A.) and microcapillary channel (Vitrocom,U.S.A.) were purchased for the magnetic levitation platform. Formlabs clear resin FLGPCL02 (Formlabs,U.S.A.) was purchased for the fabrication of magnetic levitation platform.

Glass slides was purchased from Marienfeld, Germany to bond PDMS microfluidic channels. Needles (C3 Technology, Turkey) were purchased to punch holes for fluid injection. TYGON Microbore Tubing was purchased from Cole Parmer, U.S.A. to be able to use PDMS channel in flow experiments. Red food dye (Ozmen Product, Turkey) was purchased for leakage test. Pluronic F-127, TWEEN® 20 as surfactants and Polydimethylsiloxane (PDMS) (Sylgard 184, Sigma Aldrich) for replica molding were purchased from Sigma Aldrich (U.S.A.).

Polyethylene microspheres with different densities (1.00 g/mL with size of 10–20 μm, 1.02 g/mL with size of 10–20 μm, 1.05 g/mL with size of 45–53 μm, 1.07 g/mL with size of 10–20 μm and 1.09 g/mL with size of 20–27 μm) were purchased from (Cospheric LLC., ABD). Gadavist® was purchased from Bayern, Germany to use as paramagnetic salt solution.

DMEM (Dulbecco's Modified Eagle's Medium), phosphate buffer saline (PBS), FBS (Fetal Bovine Serum), penicillin-streptomycin were purchased from Thermo Fisher, Germany. RPMI (Roswell Park Memorial Institute) 1640 was obtained from Euroclone,

Italy. Trypsin was purchased from Biological Industries. MDA-MB-231-line and U-937 cell line were kindly provided by Assoc. Prof. Dr. Engin OZCIVICI and Asst. Prof. Dr. Meltem ELITAS, respectively.

Ethanol (Merck, Germany) and 2-Propanol (VWR Int., Germany) were obtained for cleaning glass slides, silicon wafers and removing the resin.

2.1.2. Instruments

MicroWriter ML3 (Durham Magneto Optics, U.K.) mask writer was used fabricate Cr Mask. Using Spin Coater (G3P-8 SCS, U.S.A.), Silicon wafer was coated at desired thickness and mask aligner (OAI, U.S.A.) was used to expose microfluidic channels onto the Si wafer. Ultrasonic bath (Isolab, Germany) was used to clean glass slides. The incubator (Memmert, Germany) was used to cure PDMS. Oxygen (O_2) plasma (ZEPTO Diener, Germany) was used to bond PDMS microfluidic channel to the glass slide. Form Labs Form 2 3D Printer was used to fabricate the magnetic levitation platform. Syringe pump (NE-1600 New Era, U.S.A.) was used to create flow within the microfluidic channel at the desired flow rate. With using the inverted microscope (Zeiss Axio Vert A1, Germany), microparticles and cells were monitored in the magnetic levitation platform.

2.1.3. Softwares

To design the magnetic levitation platform, student version of AutoCAD 2018 was used. The necessary support parts were added to the design of maglev platform via PreForm. Based on COMSOL Multiphysics, the magnetic induction (B) between the magnets was modeled and solved. The final positions of the microparticles and cells under magnetic force, drag force and bouncy force inside the channel were calculated by MATLAB. The levitation heights of the beads and cells were determined using Image J.

2.2. Methods

2.2.1. Chromium (Cr) Mask Fabrication

Since SU-8 is a negative photoresist, the regions where the channels are defined onto the mask were transparent and harden after UV exposure. Therefore, the residual part was presented in the dark region.

Based on the obtained simulation data, the technical scheme of the photolithography mask to be used to produce the mold of the microfluidic chip was drawn by the computer-aided design program (AutoCAD 2018). The mask with four different microfluidic channel designs (Figure 2.1.) was produced at Bilkent University- National Nanotechnology Research Center (UNAM) via mask writer (MicroWriter ML®3).
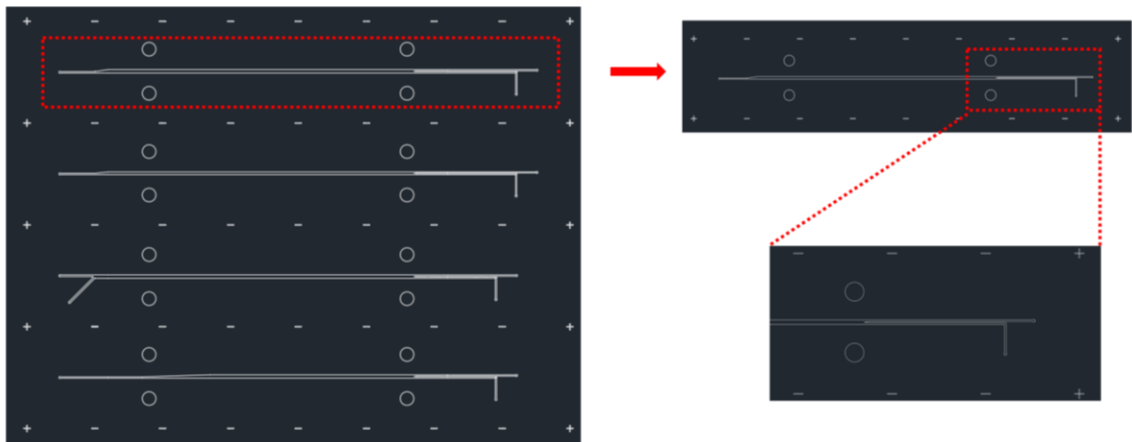
Figure 2.1. Mask Design

2.2.2. Microfabrication

The photolithography technique was used to produce microfluidic chip molds in a clean room. First, the silicon (Si) wafer was cleaned with isopropyl alcohol and then

dried with nitrogen. In order to coat the surface of the Si wafer with SU-8 50 negative photoresists, wafer attached to the rotating part of the spin coater via vacuum holder without touching the surface of the wafer. The SU-8 was poured via a Pasteur pipette onto the Si wafer and coated by the spinner. It is ensured that the resist was evenly spread homogeneously to the surface as a thin layer. The desired SU-8 thickness was 100 μm and the wafer must be rotated to find the optimum spin speed to achieve this thickness. The wafers were rotated at 2500, 3000 and 3500 rpm for 47 seconds. The SU-8 thicknesses were obtained according to these spin speeds are given in Figure 2.2. At 3500 rpm, the SU-8 thickness was measured as 100 μm and the study was continued by selecting this rotational speed.
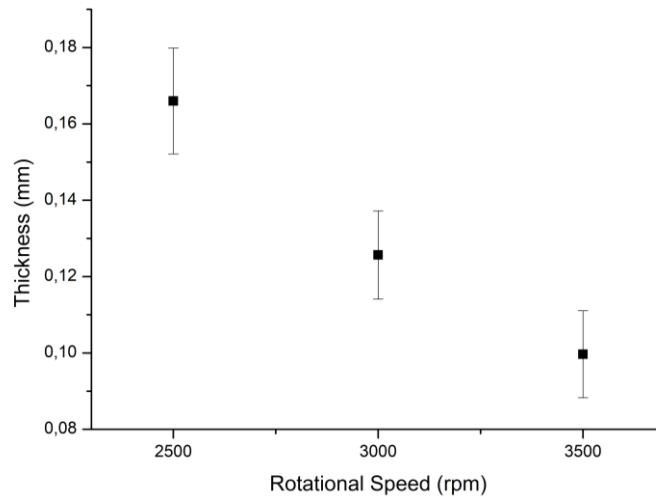
Figure 2.2. The thickness of the SU-8 resist depending on the rotation speed

Once the desired photoresist thickness on the wafer was obtained, the photoresist was hardened by removing solvents with soft bake. In this process, the Si wafer was first kept at 65 ° C for 10 minutes and then at 95 ° C for 30 minutes. Then, mask was placed on the Si wafer covered with photoresist and ultraviolet light (UV) exposed to wafer by mask aligner (OAI Mask Aligner, U.S.A.).

The Si wafer was exposed to 10 mW of UV light 5 times in 12 second periods. Following exposure, the Si wafer was subject to post expose bake. For this process, the Si plate was first kept at 65 ° C for 1 minute and at 95 ° C for 10 minutes. At the end of the treatment, the Si wafer was cooled to room temperature.

Once exposed, the development part was started to remove the resist in the areas where UV light did contact on the Si wafer and to reveal the channel patterns. In this step, the wafer was placed in a crystallization dish with propylene glycol methyl ether acetate (PGMEA) and agitated for a while and was removed from the dish and transferred to another crystallization dish containing isopropyl alcohol. If a white color is observed in the crystallization dish containing isopropyl alcohol, the wafer is taken into the dish with PGMEA and once again agitated for a while. This process was continued until the unwanted resists were completely dissolved. After dissolution, the desired patterns were created onto the wafer and the wafer was cleaned with non-ionized water and dried with dry air. Microscopic images of microfluidic channels on Si wafer produced by photolithography technique in clean room are shown in Figure 2.3.

Figure 2.3. Microscope images of the microfluidic channel master. (a) The inlet of the microfluidic channel, (b-c) The microfluidic channel, (d) The separator and (e) The dual outlets of the microfluidic channel. Scale bar shows 200 μm.

The width of the microfluidic channel was plotted as 400 μm in the AutoCAD program and the channel width produced in the clean room was 402 ± 1 μm. Considering these values, it can be said that microfabrication is successful. At the end of the process, the silicone plate was cut at National Nanotechnology Research Center (UNAM, Ankara) and four different channel designs on the wafer were separated from each other.

2.2.3. Microfluidic Chip Production Using Polydimethylsiloxane (PDMS)

After the technical drawings of the 3D printed molds which were required for the placement of the Si wafer with the SU-8 patterns on it and the formation of the channel wall thicknesses, the drawing file was saved in the appropriate format (with the extension .stl) to be printed on the 3D printer (Formlabs Form 2). Then, the necessary support parts

were added to the design with the PreForm software and the parts were ready for printing (Figure 2.4). Then, the last version of the drawing file (with the extension. form) was sent to the 3D printer and printing was started. The three-dimensional printing process was carried out using "Clear v2 FLGPCL02" photoreactive resin using a stereolithography technique with a resolution of 0.025 mm. The 3D printer completed the printing process by starting from the base with the UV laser focusing on the photopolymer resin and forming a layer by layer product.
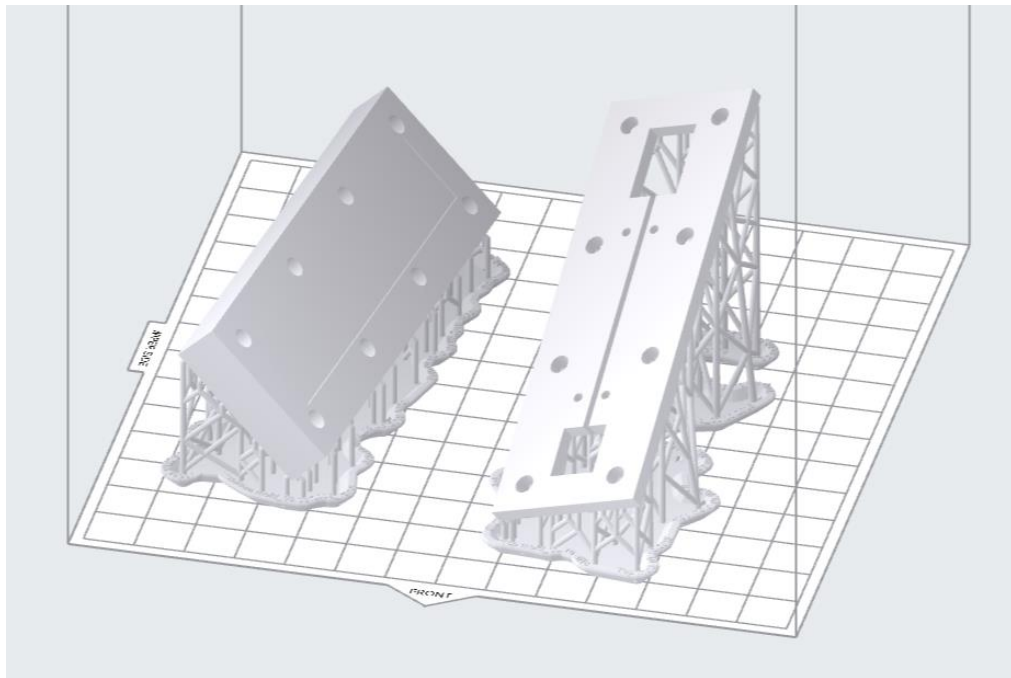
Figure 2.4. The screen of the interface used to make it suitable for three-dimensional printing by adding support parts to designed molds.

After printing process, the two printed pieces of the molds were scraped off the printer surface. According to the recommendation of the manufacturer, the printed parts were washed twice with isopropyl alcohol for 10 minutes. After treatment with isopropyl alcohol, the pieces were dried with filter paper and cut from the support parts with a pliers.

After making the molds suitable for use, the assembly was united together using 8 screws and nuts so that the silicone plate was remained in the middle of the top and bottom mold.
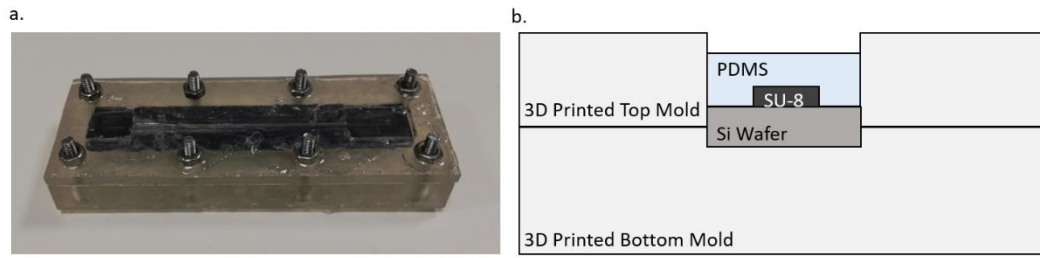
Figure 2.5. The mold of the microfluidic channel. a. The mold used for producing PDMS microfluidic chip and b. cross-section of the PDMS mold.

Polydimethylsiloxane (PDMS) is a material that commonly used for the fabrication of microfluidic devices due to its inimitable properties via soft lithography techniques. PDMS is preferred for biomedical microelectromechanical systems (BioMEMS) applications for a set of reasons: (i) optically transparent; (ii) nontoxic, biocompatible and environmentally safe ; (iii) elastomeric, conforms to smooth, non-planar surfaces; (iv) flexible and easy to mold; (v) it requires low temperatures for completely curing; (vi) deformed reversely; (vii) it might seal reversibly to itself or other material surfaces to make weak van der Waals forces (capable to keep fluid pressures about 5 psi) and can seal irreversibly by making tight covalent bonds (hold air pressures until 30-50 psi) [82-86].

PDMS Sylgard 184 was used for casting 3D printed mold. PDMS, a silicone-based elastomer, was poured into the mold to produce microfluidic chip rapidly. PDMS is a two-part polymer composed of silicone elastomer base and curing agent. Standard mixing ratio for PDMS is 10 (elastomer base): 1 (curing agent) and depending on the ratio 10:1, PDMS was prepared with enough volume for the mold and mixed until transparent. The prepared PDMS was stored in the desiccator until the air bubbles in the container were removed. The air bubble-free PDMS was slowly poured onto the silicon wafer mounted between the molds (Figure 2.5.a). The device was then put into the desiccator again to remove any air bubbles formed on the plate. Then the prepared platform was kept in the oven for 12 hours at 65 °C and the PDMS was completely hardened. The completely cured PDMS was peeled from the mold and placed on the glass surface. The PDMS molded the SU-8 patterns on the Si plate and formed the microchannel on the PDMS (Figure 2.6.) [87]. The holes for the inlet and outlet flows were drilled with (1.4 mm inner core) a pointed needle.
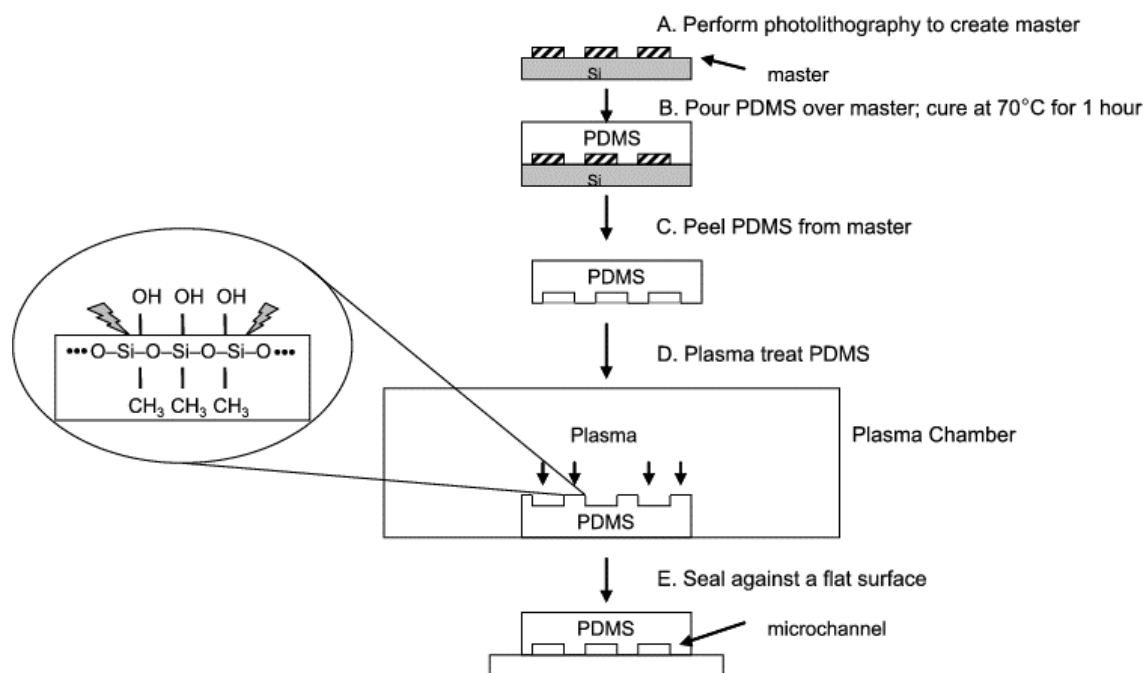
Figure 2.6. Schematic illustration of PDMS microchannel fabrication via plasma activated bonding protocol (Source: Dang et al., 2008 [87]).

2.2.4. Oxygen (O$_2$) plasma

Since unaltered PDMS has a hydrophobic surface, it is hard to wet with solutions and cannot seal with a surface of material easily [86] .PDMS polymer comprises of –O–Si (CH$_3$)$_2$– repeated units. When exposing PDMS surface to an oxygen plasma, silanol groups (–OH) were presented at the expense of methyl groups (–CH$_3$) [84, 86, 88, 89]. These covalent bonds yield the principle of an irreversible seal tightly between the layers [86, 90].

The PDMS and the glass surface were joined to enclose the bottom surface of the channel. PDMS and glass slide were prepared for oxygen plasma treatment. For that, glass slide was first cleaned with 70% ethyl alcohol (EtOH), DI water and dried with air. By way of the oxygen plasma treatment (Zepto Plasma, Diener) during 2 minutes at 100 mW was aimed to activate the surface of both pieces surface modification to provide permanent adhesion to each other. After O$_2$ plasma, the PDMS is bonded to the glass slide surface and the microfluidic chip was successfully produced (Figure 2.7) and put into the oven at 80 °C to for about 20 minutes to improve adhesion.
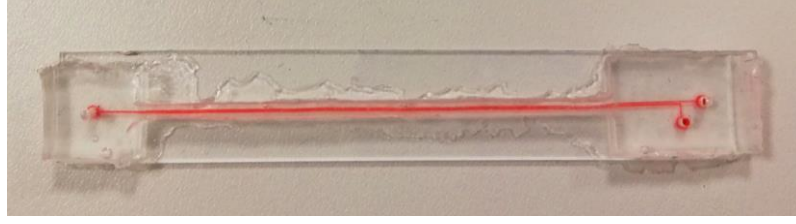
Figure 2.7. The PDMS microfluidic channel

The width of the channel produced was 400 μm. In addition, PDMS side wall thickness was measured as 450 μm for bottom side and 630 μm for the top side (Figure 2.8). These thicknesses were enough to place the magnets at measured distances used in modelling.
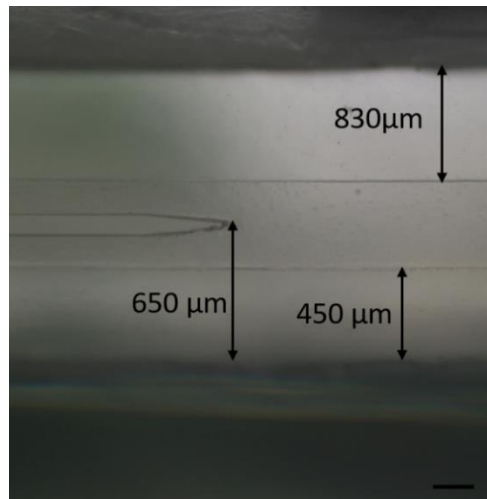
Figure 2.8. The microfluidic channel wall thicknesses and the separator height

2.2.5. Design and Manufacture of The Magnetic Levitation Device

The technical schemes for the necessary parts to assemble the main parts of the magnetic levitation platform and to display the inside of the microfluidic channel were drawn with the CAD program as AutoCAD 2018.

The setup consists of; i. the part in which the magnets are to be positioned in the desired manner (Figure 2.9.a) and then ii. the part where magnets and the microfluidic channel are to be placed (Figure 2.9.b).
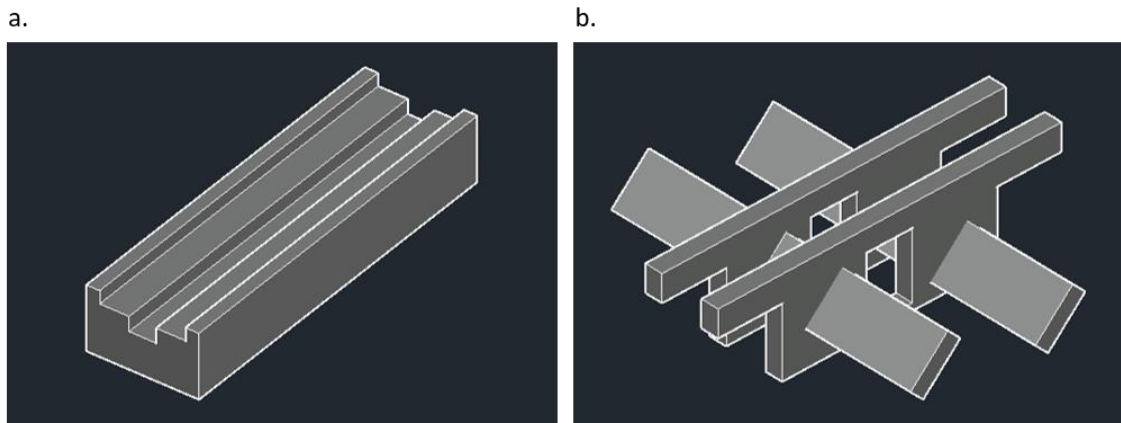
Figure 2.9. AutoCAD image of the parts used in magnetic levitation platform. a. The holding element in which the magnets and the microfluidic channel are placed and b. where the magnets are to be attached in AutoCAD.

After the printing process was completed, the printed parts were scraped off the printer surface. According to the recommendation of the manufacturer, the printed parts were stored in the reservoir for 10 minutes with isopropyl alcohol. Then again, the steps in the first step were repeated by taking it to a second chamber containing isopropyl alcohol. After treatment with isopropyl alcohol, the pieces were dried with filter paper and cut from the support parts with the pliers.

The pieces of equipment for the mechanism operating with the magnetic levitation principle; i) Four (36 x 10 x 4 mm) mirrors, ii) two neodymium N52 magnets (dimensions: 50.8 mm length $\times$ 2 mm width $\times$ 5 mm height) were provided and iii) a PDMS microfluidic channel was produced (Figure 2.10).

Various drawings have been made in order to obtain the optimum dimensions of the pieces that will be used in the construction of the assembly. In the developed platform, the dimensions of the pieces that allow to observe the levitation heights of the microparticles /cells under the microscope and the dimensions of the components which allow the platform to be assembled in the most suitable manner are determined as final dimensions.
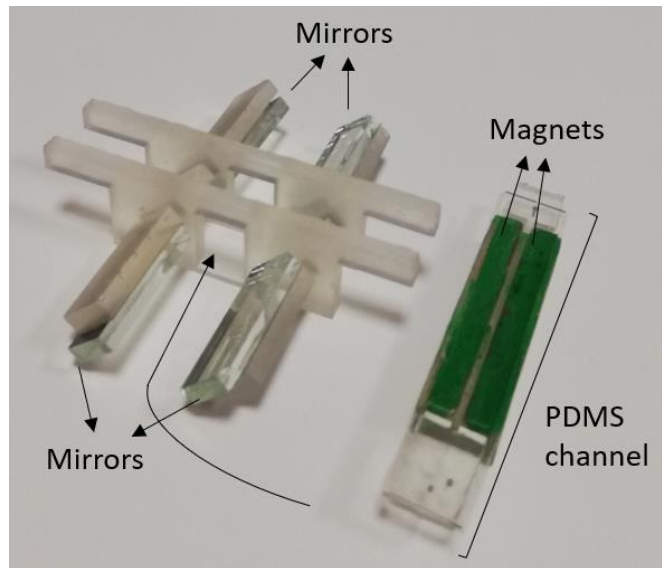
Figure 2.10. The magnetic levitation platform consisting of four mirrors, which are used for monitoring, two magnets used to create magnetic field and PDMS microfluidic channel.

In order to create a magnetic field in the microfluidic channel, the apparatus is provided that allows the magnets to be positioned with the same poles facing each other (Figure 2.9.a). This apparatus ensures the magnets to be positioned so that the distance between the magnets determined by magnetic simulations is ~ 1.5 mm. The thickness of this piece was determined to be 8.75 mm in order to prevent the deformation caused by the magnets pushing each other. Magnets are glued with epoxy to the 3D printed apparatus as the opposite poles facing each other. Then, the PDMS microfluidic chip was placed between these magnets (Figure 2.9.b) and placed in the magnetic levitation device to allow the platform for separation tests to be ready. The microfluidic chip in the platform is interchangeable and all other parts can be reused in different tests.

2.2.6. Cell Culture

MBA-MB-231 breast cancer cell line was cultured in DMEM (Thermofisher, Germany) supplemented with 10 % fetal bovine serum (FBS) and 1 % Pen-Strep at 37 °C in a humidified atmosphere with 5 % CO_2.

U-937 human monocyte cells were maintained in RPMI 1640 (EuroClone, Italy) medium containing 10 % fetal bovine serum (FBS) and 1 % Penicillin-Streptomycin (Pen-Strep) at 37 °C in the humidified atmosphere with 5 % CO_2.

2.2.7. Magnetic Levitation of The Cells

MDA-MD-231 cells that were cultured in the growth media and then were trypsinized at 37 °C for 5 min. Later, cells were centrifugated at 1100 rpm for 5 min. The pellet was resuspended to 10^5 cells per ml in the culture medium. From this concentration, cells were diluted using FBS down to 10^3 cells/mL, 10^2 cells/mL and 10 cells/mL in the culture medium containing the gadolinium (Gd $^{3+}$) paramagnetic agent as 30 mM. MDA-MB-231 cells were levitated and sorted in FBS containing 30 mM Gd concentration.

U-937 cells were cultured in RPMI-1640 growth media and then were centrifugated at 1100 rpm for 5 min. The cell pellet was resuspended to 10^7 cells/mL and 10^6 cells/mL in the culture medium. From these concentrations, cells were diluted using FBS down to 10^5 cells/mL in the culture medium containing the gadolinium (Gd $^{3+}$) paramagnetic agent as 20 mM, 30 mM and 40 mM. 10^7 cells/mL, 10^6 cells/mL and 10^5 cells/mL. U-937 cells were levitated and sorted in FBS containing different Gd concentrations.

CHAPTER 3

RESULTS AND DISCUSSION

At the beginning of the study, Finite element modelling (FEM) was used to find the optimum flow rate, Gadavist concentration and channel dimensions to achieve higher sorting efficiency. Magnets and separator of the microfluidic channel were positioned and mask were designed according to the simulation results. After modelling part, microfluidic channel and magnetic levitation platform were produced to perform sorting experiment by using beads and two different cell line.

3.1. Modeling Flow Rate and Pressure Values in the Microfluidic Channel

The flow profile in the microfluidic channel and the amount of pressure required for proposed flow were calculated by the finite element method (FEM). The flow rate was determined to be at least 1 mL/hour to separate the 1 mL cell mixture in less than 1 hour. Since 5 cm long magnets are used to separate the cells, the channel length was determined as 5 cm for the separation of the cells along the magnet. The channel height was selected to be 50 μm so that the cells (<30 μm diameter) could move without jammed through the channel. The channel width was initially determined as 400 μm in order to achieve the required height for cell separation. According to specified microfluidic channel dimensions, the flow profile formed in the channel and the amount of pressure generated in the channel during 1mL/h flow rate were analyzed by COMSOL Multiphysics modeling software. The results show that the parabolic flow profile was formed inside the microfluidic channel (Figure 3.1.a-b). This shows that the selected parameters form the laminar flow profile in the channel, the cells move on the straight flow lines, and the flow in the direction of magnetic force has no effect. A pressure drop of 2.07 Pa was observed for a channel length of 50 μm (Figure 3.1.c).
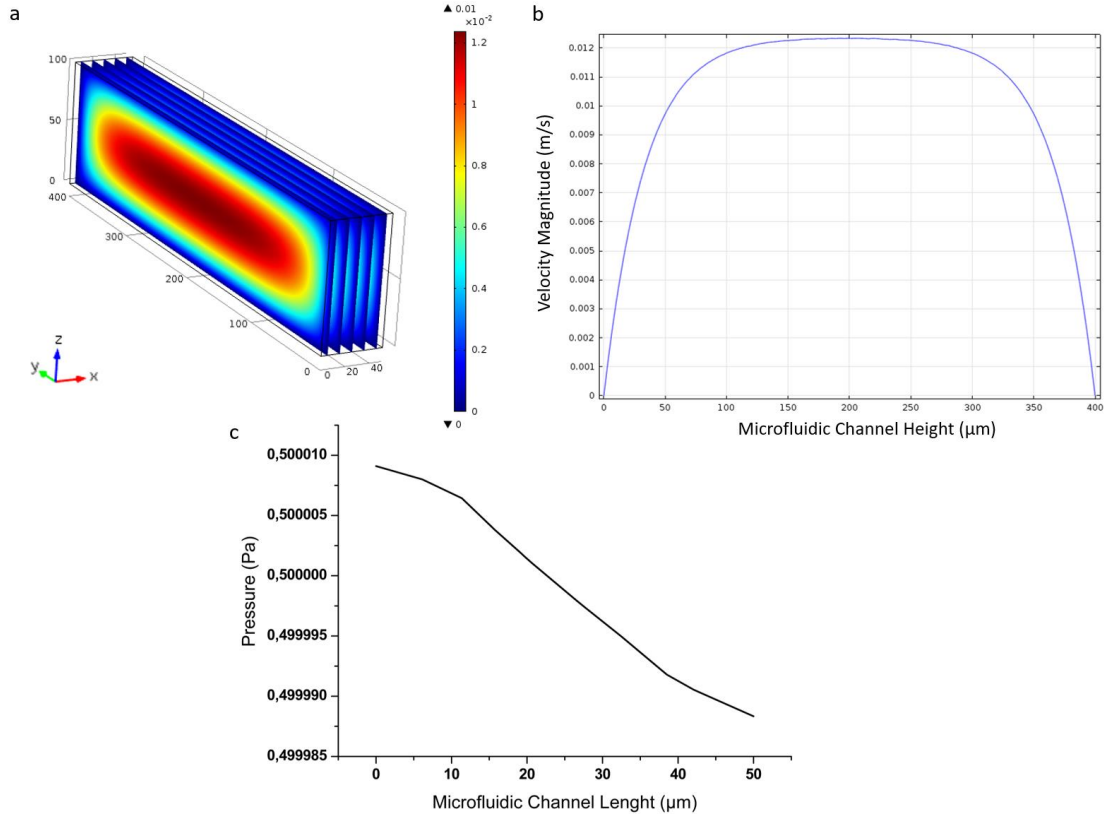
Figure 3.1 Microfluidic modeling results. a. Flow velocity profile in the microfluidic channel section, b. Parabolic flow profile in the middle of the microfluidic channel with the height of 400 μm and c. Pressure change profile through 50 μm channel length.

This pressure drop corresponds to a value of 2.90 kPa for a channel length of 7 cm. Since this value is far below the 400 kPa, which is the adhesion force of the material of the polydimethylsiloxane (PDMS) from which the microfluidic channel is produced, it is foreseen that no leakage will occur in the channel [91].

3.2. Modeling of Magnetic Induction in the Microfluidic Channel

The magnetic induction is calculated by the formula $B = \mu_0 (H + M)$. In this formulation, M is magnetization (1150 kA/m for neodymium N52 magnets), H is magnetic field and μ_0 is permeability of free space.

The microfluidic channel was placed at 0.45 mm and 0.63 mm from the bottom and top magnets, respectively. The magnetic induction resulting from these conditions was modeled with COMSOL Multiphysics software (Figure 3.2.a).
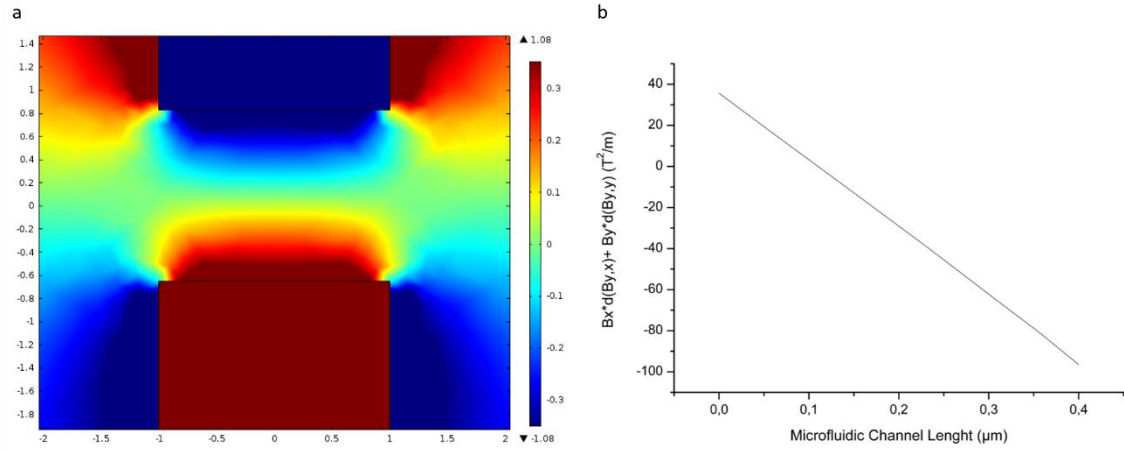
Figure 3.2. Modeling results of magnetic induction. a. Magnetic induction intensity of the microfluidic channel between two magnets and b. Variation of induction values relative to the microfluidic channel width (y axis).

3.3. Modeling of Levitation Height of Cells in Microfluidic Channel

The magnetic force acting on the cells inside the microfluidic channel was calculated by;

$$F_m = \frac{V x_m}{\mu_0} \times \left(B_x \frac{\partial B_z}{\partial x} + B_y \frac{\partial B_z}{\partial y} + B_z \frac{\partial B_z}{\partial z} \right) \tag{3.1}$$

Magnetic induction values in parentheses were determined by COMSOL Multiphysics software. This section varies linearly to the distance of the cell from the magnet (to the position above the channel width) for the proposed design (Figure 3.2.b).

Hydrostatic lifting force also affects the cells in the channel. This force was calculated as follows;

$$F_b = \Delta \rho v g = 0 \qquad (3.2)$$

Besides the magnetic force and bouncy force, the drag force;

$$F_d = 6\pi R \eta f_d v \qquad (3.3)$$

acts on the cells moving in the magnetic field. In the formula, R represents the radius of the cell, η is the dynamic viscosity of the solution, f_D is the drag coefficient (taken as 1 if away from the channel wall) and V is cell velocity.

In the magnetic levitation platform, the cells in the paramagnetic solution will move towards the midpoint of the two magnets, where the magnetic field in the channel is the lowest. During this movement, the drag force is equal to the difference between the magnetic force and the hydrostatic lifting force.

$$F_d = F_m - F_b \qquad (3.4)$$

At the position where the magnetic force is equal to the hydrostatic lifting force, the cell remains stationary. However, if a perpendicular flow is applied to the magnetic forces during magnetic levitation, the cells begin to drag (Figure 3.3).

In this study, it was aimed to sort the breast cancer cells from white blood cells. The density of the breast cancer cells and leukocytes were reported as 1.044 ± 0.018 g/mL with a radius of 8.92 ± 1.64 μm and 1.088 ± 0.005 g / mL with a radius of 4.52 ± 0.60 μm, respectively [74].
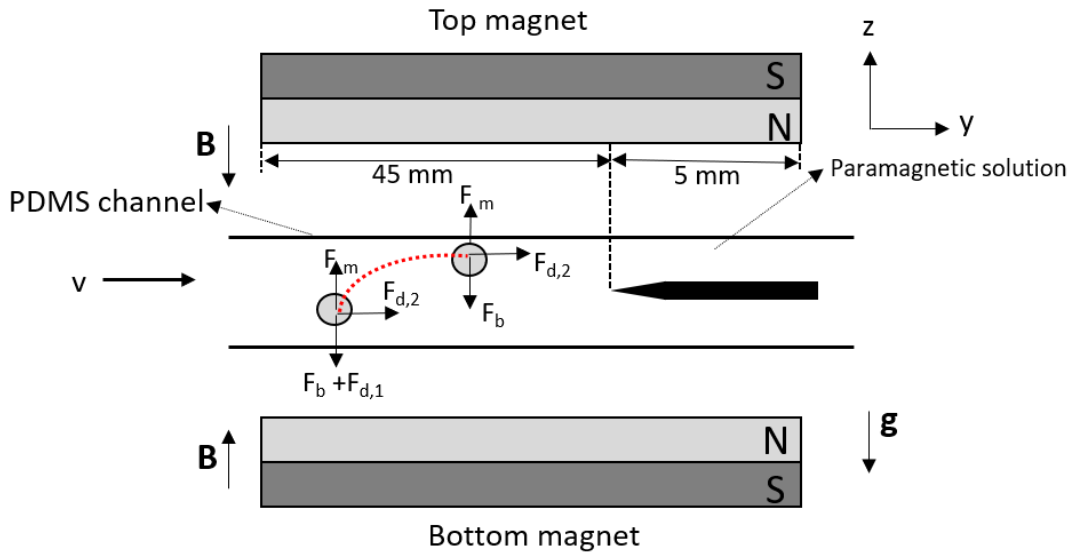
Figure 3.3 Visualization of forces acting on cells in the magnetic levitation platform. At the point where the magnetic force is equal to the hydrostatic lifting force, the cells are dragged by the flow rate v.

In order to predict the movement of the cells within the magnetic levitation platform, the cells have two different densities (1.06 g/mL and 1.09 g/mL) with diameters of 10 μm and 20 μm in 30 mM Gadavist concentration was modelled (Figure 3.4).
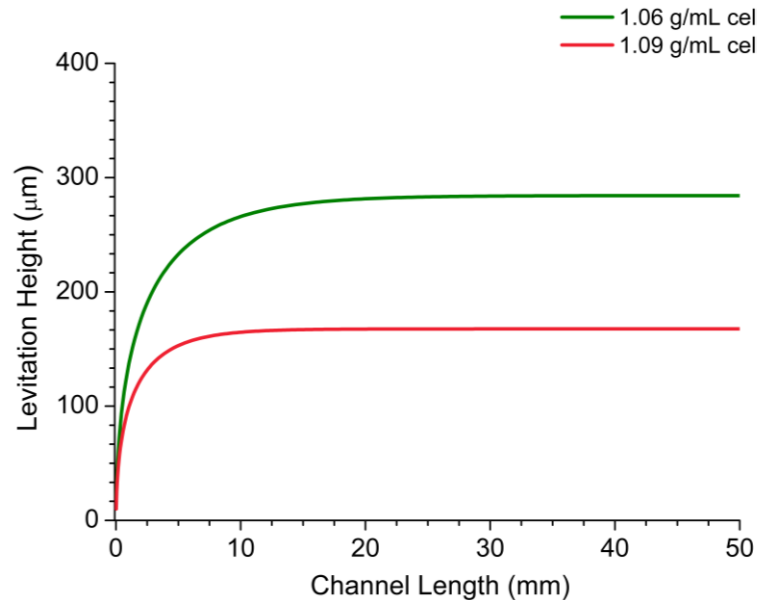
Figure 3.4. Simulated trajectories of cells obtained from the finite element modeling tool along the channel length (50 mm) according to their densities. Levitation height is represented as the distance from the bottom of the channel. The microfluidic separator is located at 200 μm height.

The magnetic susceptibility value of the Gadavist were used in the experiments was putted as 3.2×10^{-4} M^{-1} in modeling program. The velocity resulting from the magnetic lifting force with the flow velocity profile shown in Figure 3.1.b. was calculated using the 4th equation.

In simulations, it is assumed that cells spiked in 30 mM Gadavist solution are given from the (0,0) coordinate (channel length, levitation height), which is one of the farthest point from the separator. The cells were started at the bottom of the channel and the position of the cells in 1 second intervals and accordingly the magnetic induction and flow velocity values were calculated. The calculation results are shown in Figure 3.4.

3.4. Pressure Tests Applied to Microfluidic Channel

For the chip to be effectively used in the cell sorting process, it was controlled by making leakage test. For this purpose, firstly a 5 mL syringe was taken with a red food dye (Ozmen product, Turkey) and then it was inserted into the syringe pump (NE-1600 New Era Pump Systems). The syringe was attached to the chip by a flexible tubing (TYGON, Cole Parmer, U.S.A.) and after the chip was placed onto the microscope system (ZEISS Axio Vert A1) and the leaks on the chip were monitored with the 5x objective and camera. The prepared device was shown in Figure 3.5.

Figure 3.5. The flow setup consisting of the microfluidic chip, the syringe pump and the microscope

The food stain was injected to the microfluidic channel starting from at 1 mL/h flow rate up to maximum 200 mL/h, which was supported by the syringe pump. The microscope photographs under the flow of the chip were shown in Figure 3.6. There was no leakage in this flow range. Finally, the chip was tested for 1 hour with a flow rate of 2 mL/h and no leakage was observed. The desired flow rate on chip (> 1 mL/h) can be safely applied up to 200 mL/h.
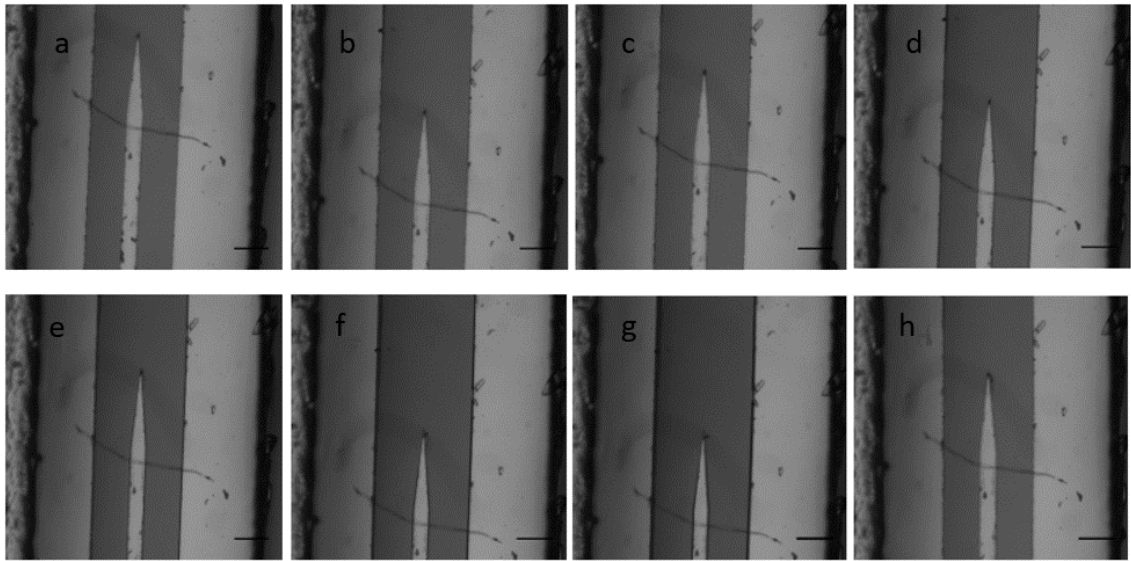
Figure 3.6. Microscope images at different flow rates of the microfluidic channel. Image of the microfluidic channel under a flow rate of a. 1 mL/h, 5 mL/h, c. 10 mL/h, d. 50 mL/h, e. 100 mL/h, f. 150 mL/h, g. 200 mL/h, h. 200 mL/h after 1 hour. Scale bar shows 200 μm.

3.5. Experiments with Microparticles in a Capillary Channel and a PDMS channel in the Magnetic Levitation Platform

To validate the simulation results, polyethylene beads with different densities (1.00 g/mL, 1.02 g/mL, 1.07 g/mL and 1.09 g/mL) spiked into the capillary channel and PDMS microfluidic channel at the magnetic levitation platform. After the manufacturing of the magnetic levitation platform, preliminary levitation tests were started in glass capillary channels (1 mm × 1 mm × 50 mm).

For the experiments, 10-27 μm sized microparticles (Cospheric LLC, USA) with different densities were used. These microparticles were prepared in Tween-20 surfactant solution because they can be easily aggregated with each other.

3.5.1. Interaction of Microparticles with The Surface of The Capillary Channel

To be able to observe unwanted adhesion of microparticles on the surface of the channel and in order to measure the effectiveness of the surfactant on these unwanted adhesions, two magnet assemblies were used in the horizontal position (Figure 3.7). Thus, the microparticles tended to aggregate in the paramagnetic solution in the middle of the magnets, regardless of their densities. Some of the microparticles will remain in air and some will be collected on the surface of the capillary by gravity.
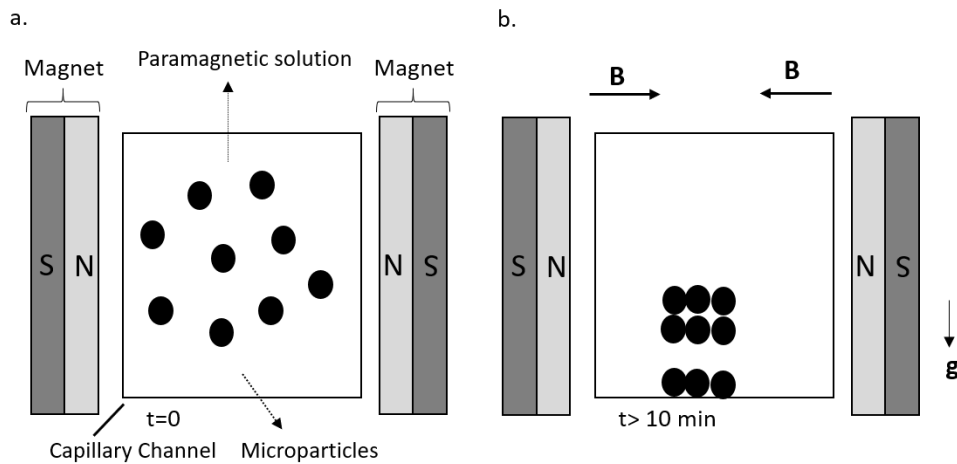
Figure 3.7. Working principle of horizontally positioned maglev device. a. The depiction of microparticles which are concentrated in the paramagnetic solution at the moment when they are placed on the magnetic levitation platform and b. Collecting the microparticles in the center of the magnets over time. The gravitational acceleration (g) is in an upright position relative to the magnetic field (B) formed in the device. The particles exposed to magnetic and hydrostatic lifting forces are collected at the midpoint of magnets over time (> 10 min), on the surface of the channel or in a suspended state.

For these experiments, fluorescent microparticles with 1.09 g/mL density were mixed with phosphate-buffered saline (PBS) containing 2 % Tween-20 and 10 % Tween-

20, followed by Gadavist paramagnetic solution containing gadolinium ion (Gd) at a concentration of 30 mM. The microparticles were then loaded into the capillary channel and placed between the magnets. After, the setup was placed on the bright field microscope system, monitored with a 5 × objective and camera. (Figure 3.8 and 3.9).
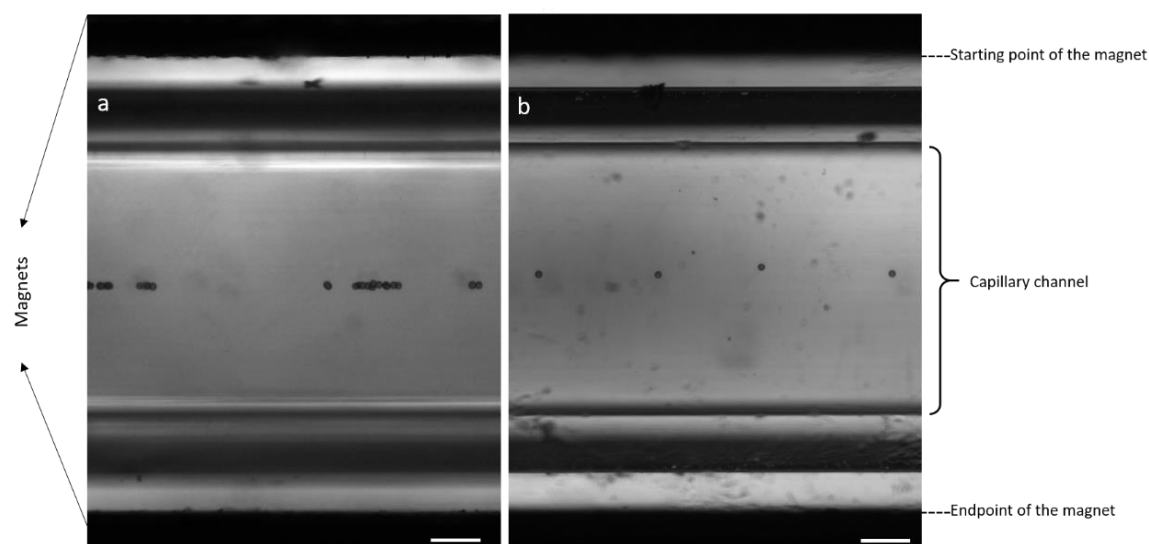
Figure 3.8. Image on the magnetic levitation setup of microparticles in 2 % Tween-20 and 30 mM Gd containing medium at 10 min. a. Images of microparticles suspended in the channel and b. collected on the surface of the channel. The scale bar shows 200 μm.
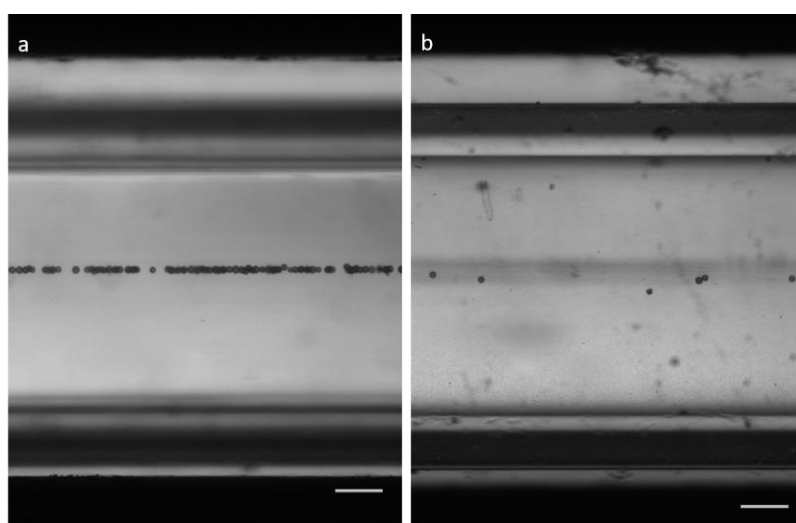
Figure 3.9. Images on the magnetic levitation setup of microparticles in 10 % Tween-20 and 30 mM Gd containing medium at 10 min. a. Images of microparticles suspended in the channel and b. collected on the surface of the channel. The scale bar shows 200 μm.

Image J program was used to analyze the coordinates where microparticles were located in the capillary channel and the microfluidic channel. Firstly, after the images taken by the microscope camera were saved with the (.JPG) extension, the recorded files were transferred to the computer to be analyzed and opened in Image J program. Capillaries containing microparticles were selected using the rectangular selection tool in the program, this section was cropped and the background was subtracted. Then, the threshold values were applied to the pixels representing the microparticles and their size and circularity parameters were restricted, and the locations and distributions of the microparticles in the channel were determined.

The locations of the microparticles relative to the middle point of the two magnets were showed in Figure 3.10. In 2 % and 10 % Tween-20 solution, the distribution of microparticles on the surface of the capillary was measured as 12.06 ± 79.53 μm and -16.22 ± 83.98 μm respectively and the locations of the suspended microparticles were 0.001 ± 13.81 μm and 11.12 ± 11.76 μm, respectively. In all cases, the microparticles were approximately collected at the middle of the magnets.
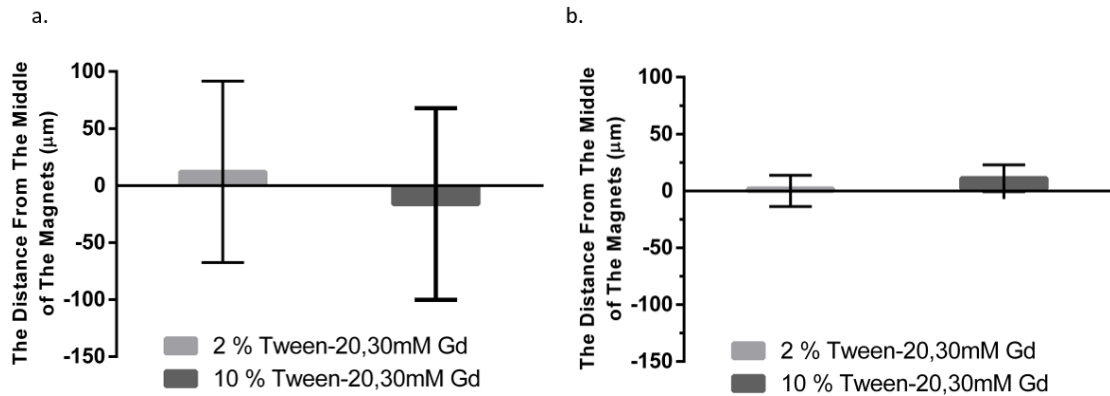
Figure 3.10. Distances of microparticles concentrated with 2 % Tween-20 or 10 % Tween-20 in a 30 mM Gd containing solution at 10 minutes in the magnetic levitation setup. The average distance of microparticles a. collected on the surface of the channel and b. suspended in the capillary was shown as a bar graph and the error bars indicate the standard deviation. The microparticle positions were shown as positive if they were above the middle point of the magnets and as negative values if they were below.

However, the distribution of microparticles collected on the surface of the channel was wide and the standard deviations were higher than the microparticles which were

suspended. This can be explained by the interaction of microparticles with the capillary channel surface. This interaction could not be reduced by increasing the concentration of Tween-20 surfactant. Since this interaction was determined to reduce the separation purity and efficiency during the separation processes, more effective surfactants were used i.e. Pluronic F-127 (Sigma Aldrich, Germany) [92, 93].

To be able to observe unwanted adhesion of microparticles on the surface of the capillary channel and in order to measure the effectiveness of the chosen surfactant, F-127 Pluronic, on these unwanted adhesions, two magnet assemblies were used in the horizontal position (Figure 3.7). For these experiments, fluorescent microparticles that have 1.09 g/mL density were mixed with a 1 % Pluronic F-127 containing surfactant in a phosphate buffered solution (PBS) followed by 30 mM Gd concentration. The microparticles were then loaded into the capillary channel and placed between the magnets. The magnetic levitation setup was then placed on the bright field microscope system and monitored with the 5 × objective and the camera (Figure 3.11).
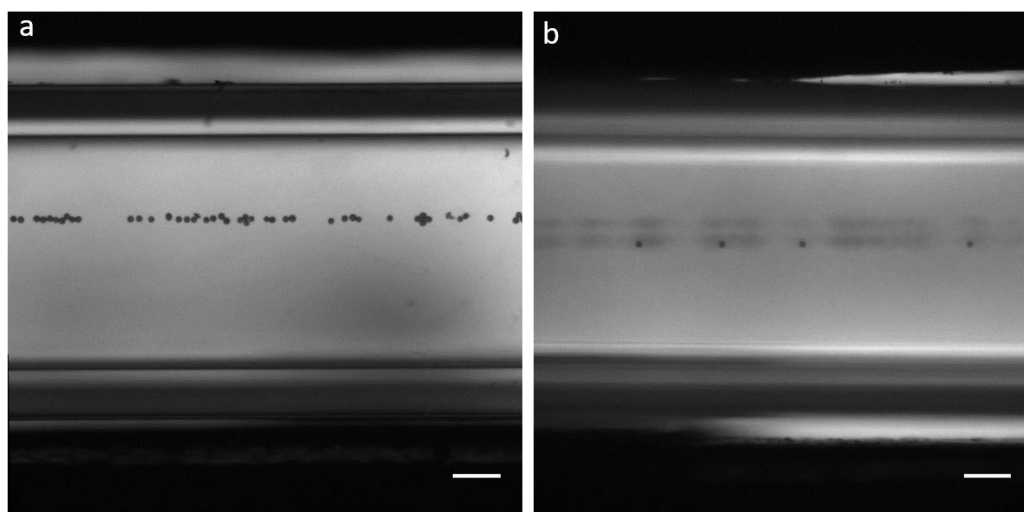
Figure 3.11. Images of the microparticles on the magnetic levitation platform in 1% Pluronic and 30 mM Gd containing medium at 10 min. Microparticles a. suspended in the capillary channel and b. collected on the surface of the capillary channel. The scale bar shows 200 μm.

In the 1 % Pluronic solution, the distribution of microparticles on the surface of the capillary channel was measured as 49.13 ± 5.20 μm whereas the suspended microparticles were measured as 0.127 ± 13.08 μm (Figure 3.12).
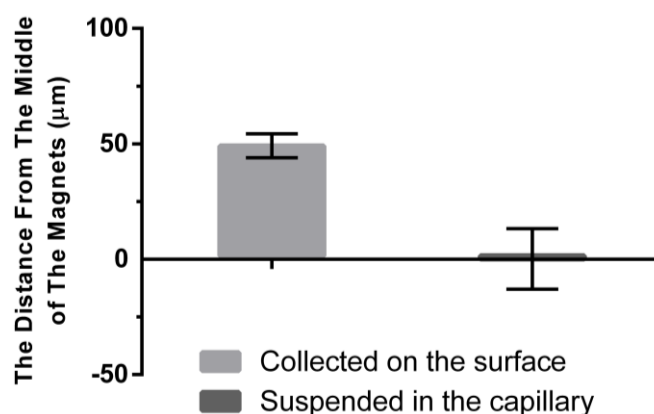
Figure 3.12. Distances of 1% Pluronic-concentrated microparticles in the 30 mM Gd containing solution to the midpoint of the magnets at 10 min in the magnetic levitation platform. The average distance of microparticles collected on a. the surface of the capillary channel and b. suspended in the capillary was shown as a bar graph and the error bars indicate the standard deviation. The microparticle positions were shown as positive if they were above the middle point of the magnets and as negative values if they were below.

In this experiment, microparticles were collected approximately at the middle of the magnets. As shown in previous experiments, the distribution of microparticles on the channel surface in the 2 % and 10 % Tween-20 solution was found to be 12.06 ± 79.53 μm and -16.22 ± 83.98 μm respectively, while the positions of the suspended microparticles were 0.001 ± 13.81 μm 11.12 ± 11.76 μm, respectively (Figure 3.10). In experiments with Pluronic, microparticles were less dispersed than Tween-20 because they remained non-stick on the surface of the channel. In order to prevent the adhesion of microparticles (and cells) to the surface, it was decided to use Pluronic in separation experiments.

3.5.2. Interaction of Microparticles with The Surface of The Microfluidic Channel

The interactions of the microparticles with the microfluidic channel surface were visualized using the horizontally positioned magnetic levitation platform (Figure 3.13.a). The bottom wall of the microfluidic channel was considered as 0 μm and then analyzed. In the solution containing 10 % Tween-20 and 30 mM Gd, 1.09 g/mL density particles

were located at a height of 257.15 ± 44.86 μm from the bottom wall of the channel (Figure 3.13.b). It is thought that the standard deviations of the microparticles in the PDMS channel were higher than those of the microparticles suspended in the capillary channel (Figure 3.10) due to the direct contact of the microparticles with the PDMS surface.
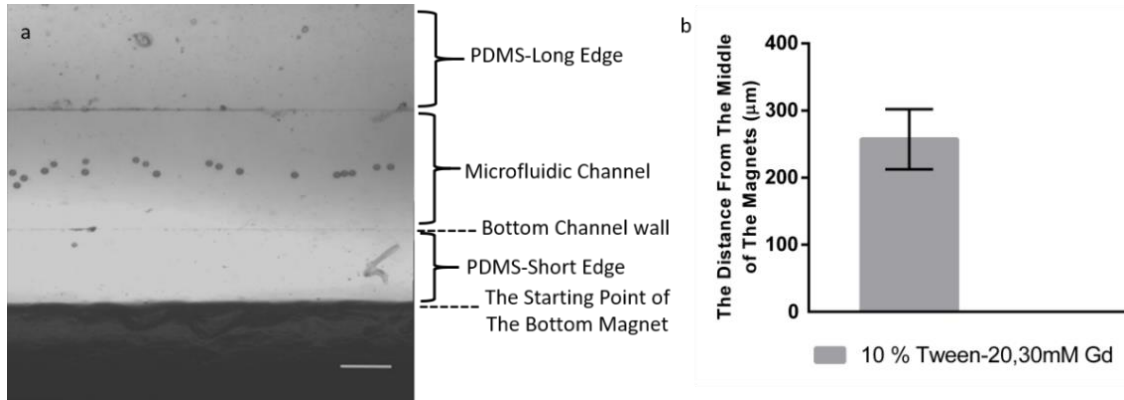
Figure 3.13. 1.02 g/mL microparticles in a 10 % Tween-20 and 30 mM Gd on the maglev platform. a. microscopic image of microparticles (scale bar is 200 μm) and b. the distance of microparticles to the bottom wall of the channel (column represent the mean height of the microparticles, error bar indicates standard deviations).

3.5.3. Magnetic Levitation of Microparticles Inside the PDMS Channel

The vertically positioned magnetic levitation platform (Figure 3.14) was used to determine the levitation performances of the microparticles in the microfluidic channel. The effect of the different Tween-20 and Gd concentrations on the levitation positions of the microparticles in the channel was analyzed (Figure. 3.15). The locations of the microparticles were calculated by accepting the bottom wall of the microfluidic channel as 0 μm. 1.09 g / mL density microparticles were precipitated on bottom wall of the channel in 2% Tween-20 and 30 mM Gd containing media.

The microparticles reached the equilibrium at a height of 108.76 ± 74.31 μm in the medium containing 10 % Tween-20 and 30 mM Gd, in the medium containing 10 % Tween-20 and 50 mM Gd at a height of 150.71 ± 65.11 μm and in the medium containing 10 % Tween-20 and 100 mM Gd at a height of 206.60 ± 78.79 μm (Figure 3.16).
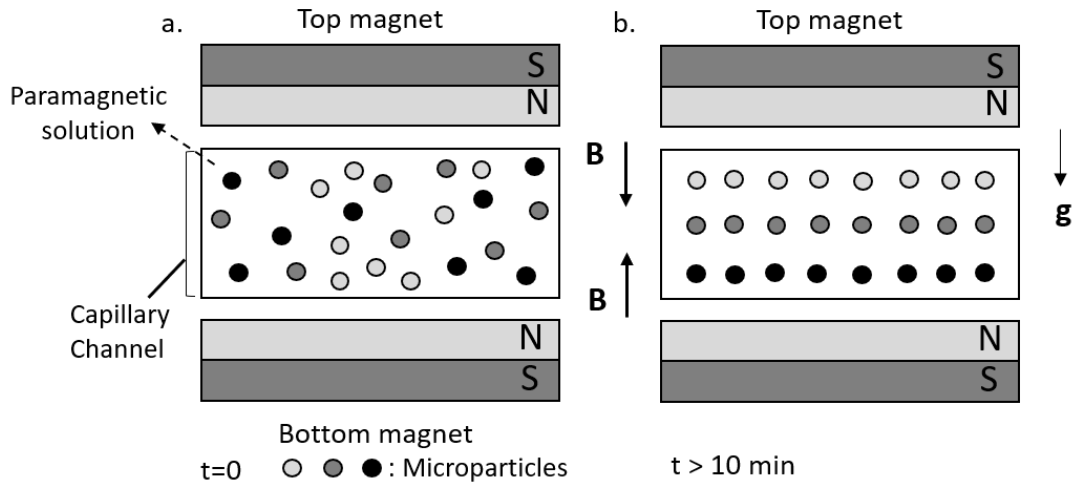
Figure 3.14. The working principle of vertically positioned maglev platform [94]. a. The depiction of microparticles which are concentrated in the paramagnetic solution at the moment when they are placed on the maglev platform and b. the different levitation heights of microparticles according to their densities. The gravity acceleration (g) is parallel to the magnetic field (B) formed in the maglev device. The particles exposed to magnetic and hydrostatic lifting forces become equilibrated in a certain plane over time (> 10 min).
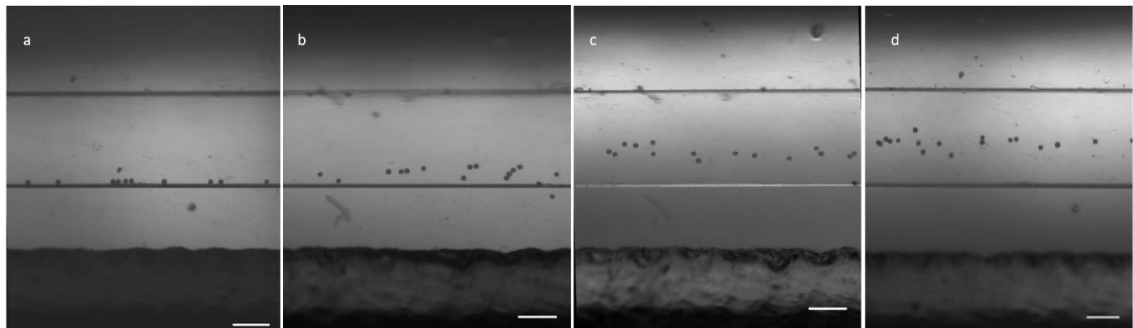
Figure 3.15. Levitation images of 1.09 g/mL microparticles in vertically positioned magnetic levitation platform in media containing different concentrations of Tween and Gadavist at 10 min. (a) in medium containing 2 % Tween-20 and 30 mM Gd, (b) in medium containing 10% Tween-20 and 30 mM Gd, (c) in medium containing 10 % Tween-20 and 50 mM Gd and (d) in media containing Tween-20 and 100 mM Gd, levitation images of microparticles. Scale bars shows 200 μm.

When the concentration of Tween-20 was increased in the experiments, the microparticles were equilibrated in the higher position in the channel because of the increase in the density of the solution containing microparticles. In addition to this, when Gd concentration was increased and microparticles were collected in higher position.
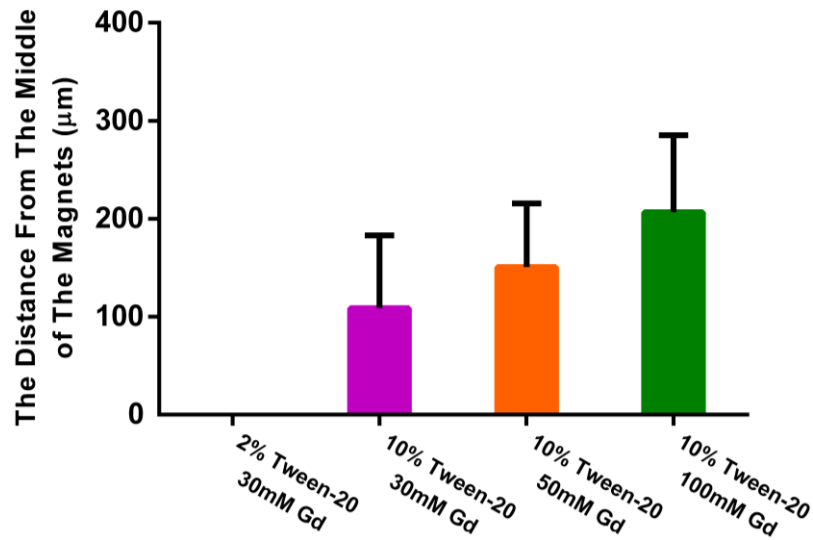
Figure 3.16. The levitation heights in solution containing 1.09 g/mL density microparticles concentrated in 2 % Tween-20 or 10 % Tween-20 with 30 mM, 50 mM and 100 mM Gd. The levitation heights of the microparticles were calculated according to their distance from the bottom wall of the channel after 10 minutes in the microfluidic channel. The columns show the average levitation height of the microparticles, the error bars indicate the standard deviation.

1.02 g/mL density microparticles could levitate in the microfluidic channel (Figure 3.17.a). In the medium containing 10 % Tween-20 and 30 mM Gd, the microparticles were located at a height of 315.42 ± 49.30 μm (Figure 3.17.b).
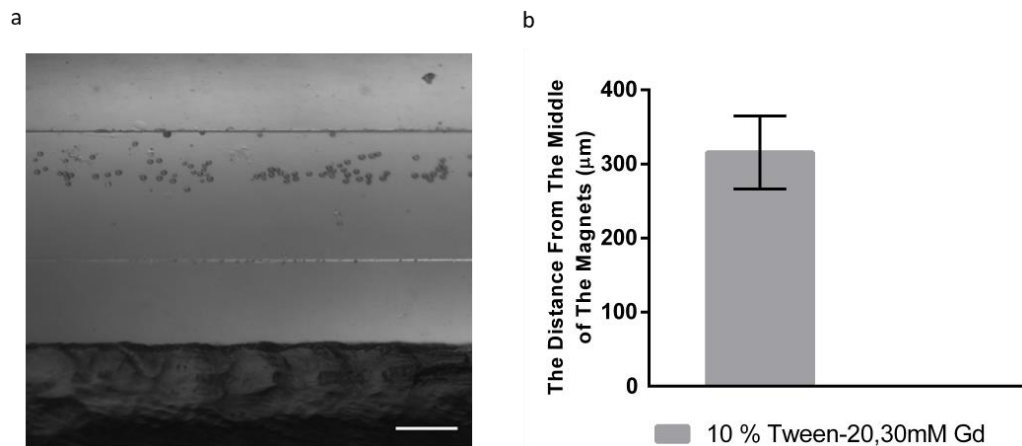
Figure 3.17. In the medium containing 10 % Tween-20 and 30 mM Gd on the vertically positioned maglev platform. a. the microscope image of 1.02 g/mL density microparticles and b. averages of their distance from the bottom wall of the channel. The scale bar shows 200 μm.

The collection of 1.02 g/mL and 1.09 g/mL density microparticles at different levitation heights was used to separate these two particles from each other. Namely; when these microparticles mixed with each other are given to the levitation platform, the 1.02 g/mL density particles were at the top of the channel, while the 1.09 g/mL density particles were at the bottom of the channel (Figure 3.18).
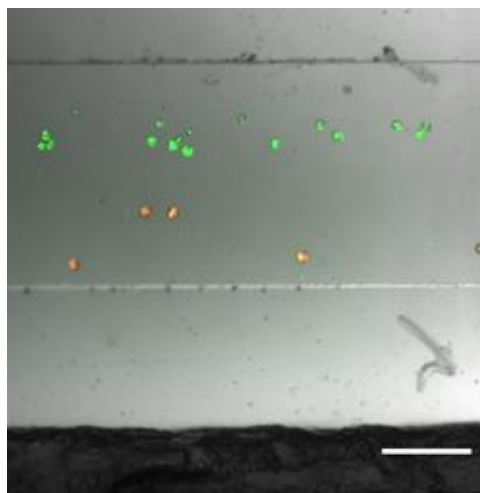
Figure 3.18. Levitation image of fluorescent microparticles having 1.02 g/ml density (green) and 1.09 g/ml density (orange) in 10 % Tween-20 and 30 mM Gd containing medium on the vertical magnetic levitation platform at 10 min. The scale bar shows 200 μm.

3.6. Determination of The Density of Microparticles

The magnetic levitation device was used in the vertical position in order to measure the density of the microparticles to be used in the sorting experiments (Figure 3.14). In the experiments, 1 g/mL, 1.02 g/mL, 1.05 g/mL, 1.07 g/mL and 1.09 g/mL density microparticles were used. The microparticles were prepared in solutions containing 0.33 % Pluronic and 15, 30, 45 and 60 mM Gadavist.

The prepared solution was loaded into the capillary channel via a pipette and then placed between two magnets. This platform was placed in the bright field microscope system and the capillary channel was monitored with the camera using the 5 × objective depicted in Figure 3.19.
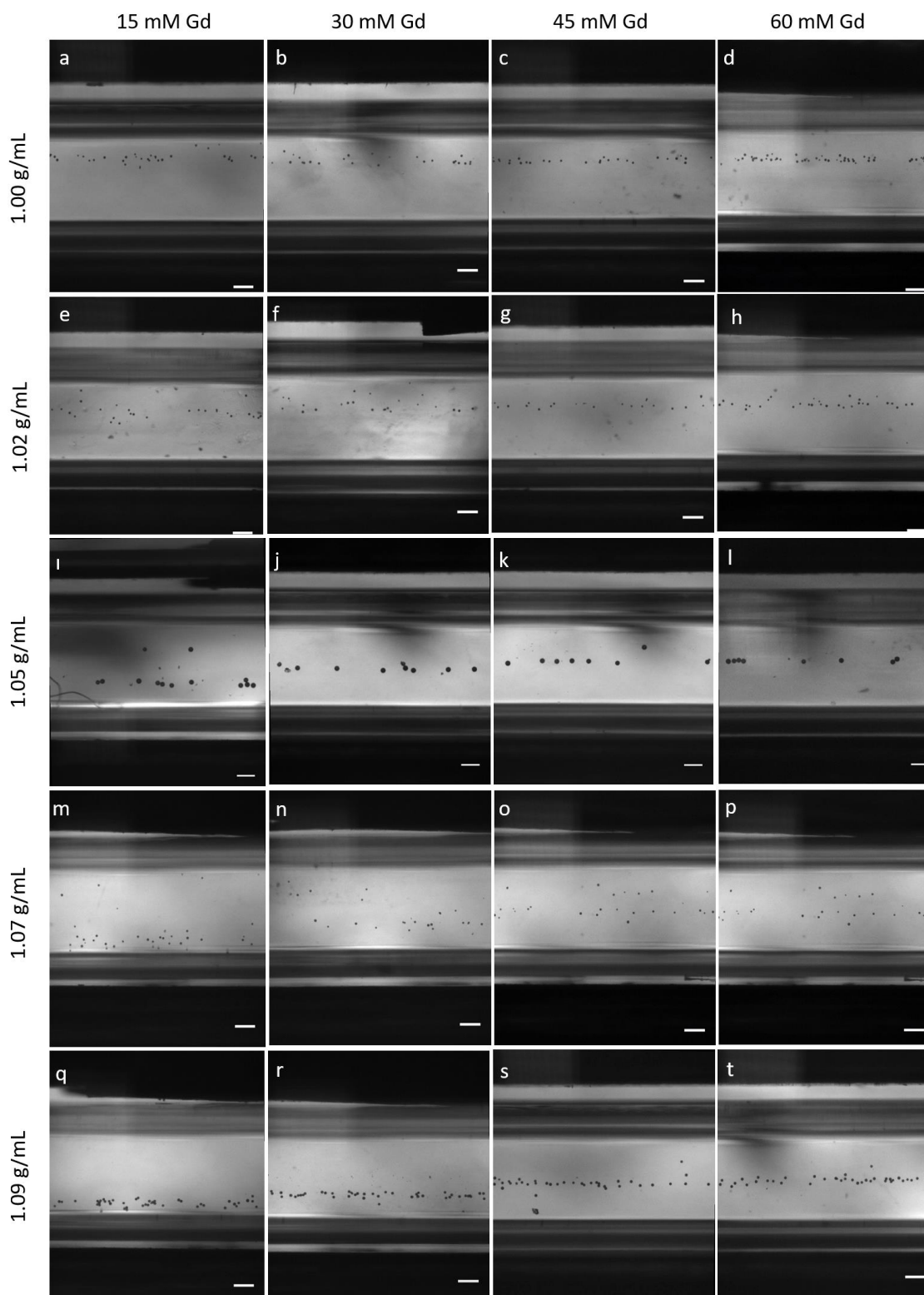
Figure 3.19. Microscopic images of the 1.0 g/mL, 1.02 g/mL, 1.05 g/mL 1.07 g/mL and 1.09 g/mL density particles in solutions containing 15, 30, 45, and 60 mM on the magnetic levitation platform, respectively. Microscope images of a-d. 1.00 g/mL density particles, e-h. 1.02 g/mL density particles, i-l. 1.05 g/mL density particles, m-p. 1.07 g/mL density particles and q-t. 1.09 g/mL density particles. The scale bar shows 200 μm.

Since the magnetization properties of the microparticles in the platform are lower than the paramagnetic solution in which they are present, they are pushed by the magnetic forces acting on them and move towards the middle of the two magnets where the magnetic field is minimum. Also, hydrostatic buoyancy force has an impact on the microparticles. At the position where the magnetic force is equal to the hydrostatic lifting force, the microparticles remain suspended (Figure 3.14).

The plane they are hanging depends on the density of the microparticles. Namely; at the bottom of the capillary channel collects high-density particles, while at the top of the capillary, low-density particles are collected.

The linear relationship between the average positions of these microparticles and their density was observed (Figure 3.20). Thus, by looking at the position of the microparticles, density determination can be made (Figure 3.21). According to the position where the microparticle is suspended, the density was determined.
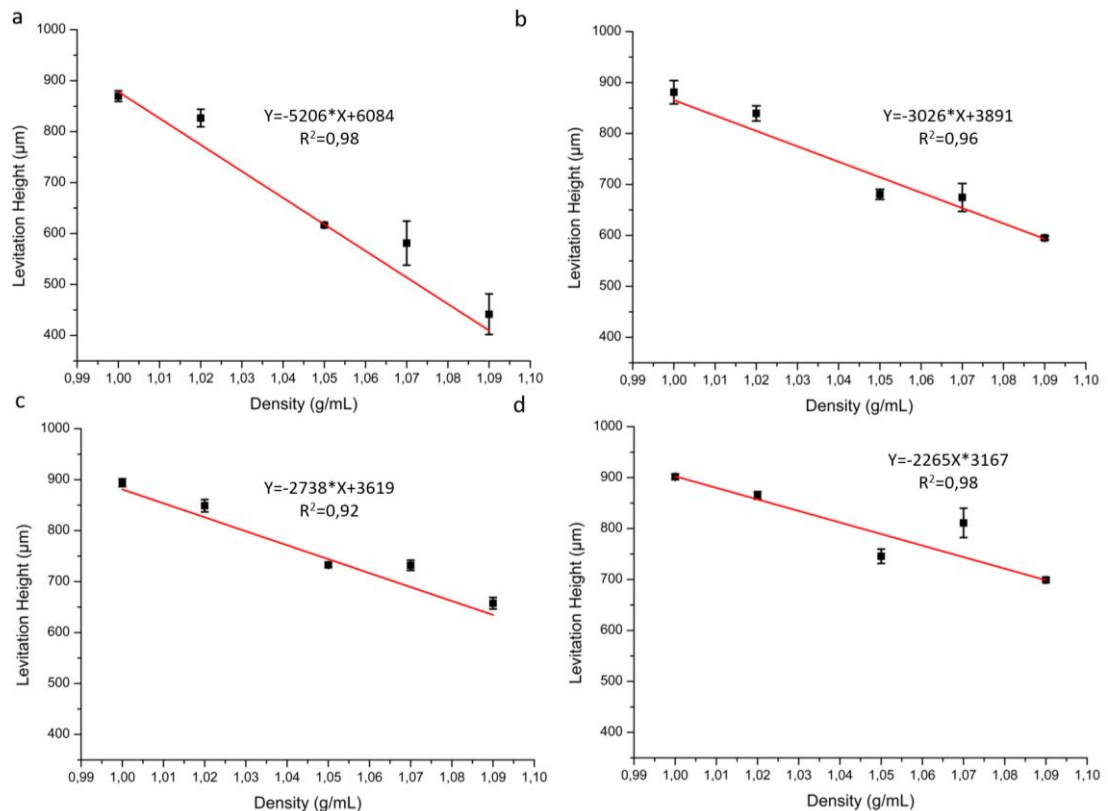
Figure 3.20. Magnetic levitation heights of different density microparticles. a. in 15 mM, b. in 30 mM, c. in 45 mM and d. in 60 mM Gd concentrations and their linear relations with their densities.

The equation of the linear curve obtained using levitation heights in 30 mM Gd containing medium of microparticles of different density is y = -3026x + 3891. In this equation, y shows the levitation height (distance from the upper limit of the bottom magnet) of microparticles in µm and x shows the density of microparticles (g/mL). Using this equation, the density of 1.00 g/mL, 1.02 g/mL, 1.05 g/mL, 1.07 g/mL and 1.09 g/mL microparticles were found to be 1.005 ± 0.009 g/mL, 1.016 ± 0.02 g/mL, 1.056 ± 0.01 g/mL, 1.066 ± 0.0407 g/mL and 1.089 ± 1.09 g/mL, respectively (Figure 3.21).
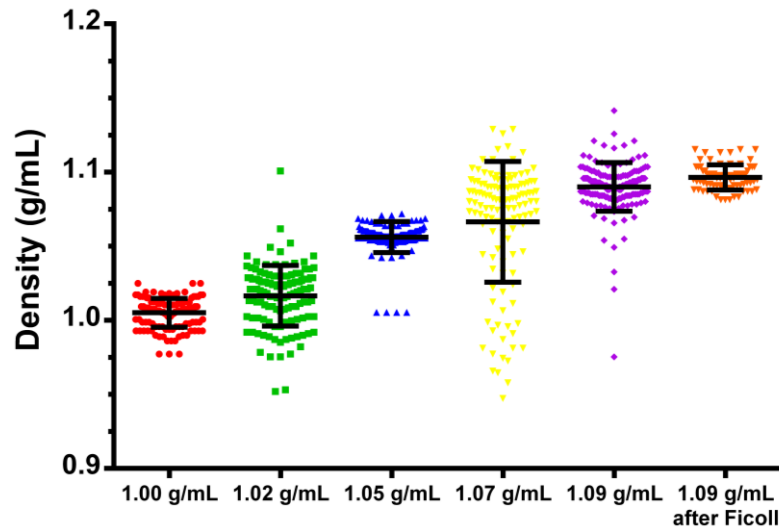
Figure 3.21. The density distribution of the different density microparticles in 30 mM Gd.

The diameters of these 1.00 g/mL, 1.02 g/mL, 1.05 g/mL, 1.07 g/mL and 1.09 g/mL microparticles were measured as 16.97 ± 3.76 µm, 18.76 ± 3.91 µm, 48.35 ± 5.97 µm, 17.79 ± 4.68 µm and 24.35 ± 4.01 µm, respectively (Figure 3.22). However, the density and diameter distributions of these microparticles were 0.977-1.024 g/mL and 9.81-26.16 -26 µm for 1.0 g/mL, 0.952-1.100 g/mL and 9.81-29.43 µm for 1.02 g/mL, 1.005-1.07 g/mL and 34.54-93.43 µm for 1.05 g/mL, 0.927-1.128 g/mL and 9.79-32.7 µm for 1.07 g/mL, 0.975-1.411 g/mL and 9.80-40.51 µm for 1.09 g/mL. Levitation height does not correlate with microparticle size. As the diameter increases, the microparticles reach the levitation height more quickly. As it is seen, these microparticles, which are used in the study and are the only standard density microparticles on the market, show a very large density distribution. To verify this observation, 1.09 g/mL microparticles were purified using the Ficoll (PM 400, Sigma) density gradient method.
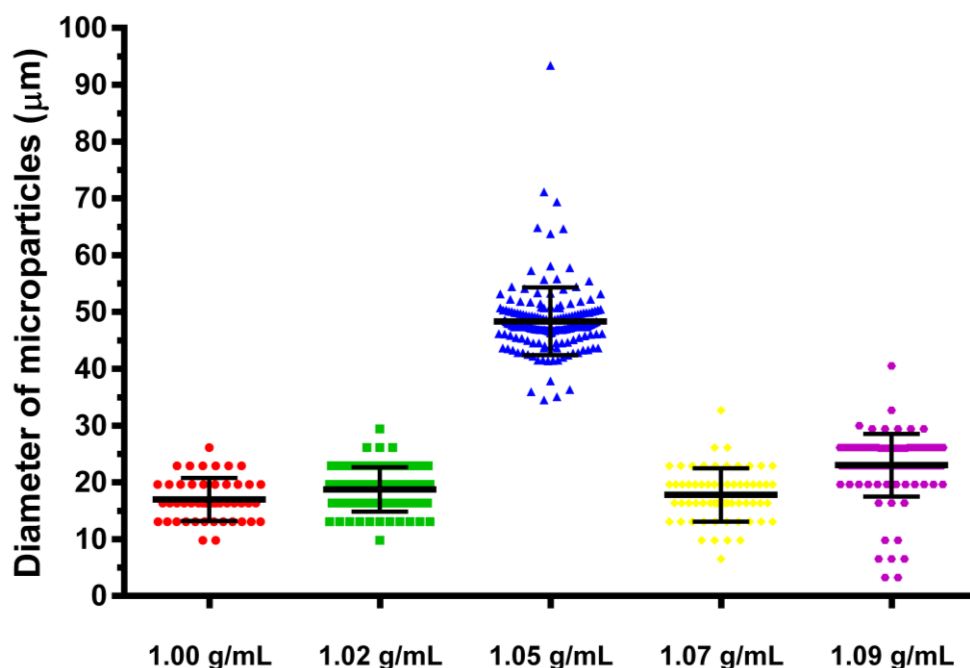
Figure 3.22. The diameter distribution of the different density microparticles

Ficoll was dissolved in PBS to provide a 50 % mass-volume (w/v) ratio and its density was determined as 1.17 g/mL with a pycnometer. The density of the Ficoll solution was reduced from 1.17 g/mL to 1.085 g/mL in order to obtain the microparticles that have 1.085 g/mL density or higher than 1.085 g/mL density. Then, 400 µL of Ficoll with a density of 1.085 g/mL was taken into the centrifuge tube and 20 µL of 1.09 g/mL microparticles in 1 % Pluronic were added. It was then centrifuged at 10000 rpm for 30 minutes. After centrifugation, the supernatant was removed by pipette. 1 % Pluronic solution was added in 1 mL of PBS on the microparticles at the bottom of the centrifuge tube, centrifuged at 10000 rpm for 15 minutes and the solution was removed by pipette. This removing process was repeated 2 times. Then 200 µL of 1 % Pluronic solution was added to the microparticles remaining at the bottom of the centrifuge tube. Thus, the density microparticles purified using the Ficoll density gradient method are expected to be greater than ~ 1,085 g/mL.

After purification, the microparticles were analyzed for levitation heights in media containing 30 mM Gd (Figure 3.23) and the density of these particles was found as 1.09 ± 0.008 g/mL.

Their distribution was 1.083-1.11 g/mL (Figure 3.21). Prior to purification, the distribution of the microparticles were reduced to 0.975 g/mL, whereas after the

purification, the density of microparticles was starting at 1.083 g/mL and were very close to the desired density value of ≥1.085 g/mL by purification. This shows the success of the purification protocol and the sensitivity of our self-mass measurement method.
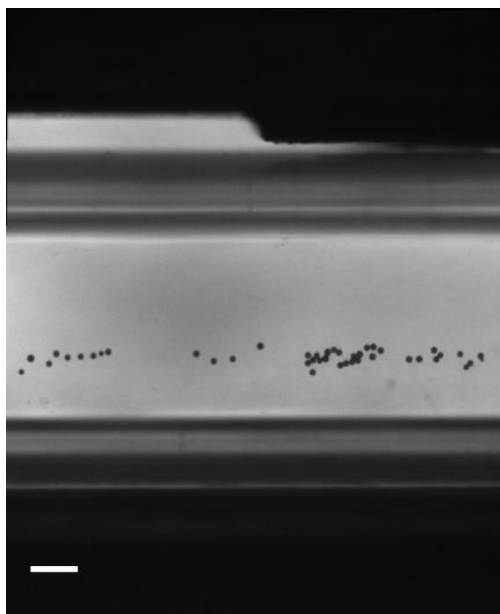
Figure 3.23. Microscope image of 1.09 g/mL microparticles purified in the desired density by Ficoll density gradient method in a capillary channel placed in the magnetic levitation platform in a medium containing 30 mM Gadavist. The scale bar shows 200 μm.

The magnetic levitation device was used in the vertical position in order to measure the density of the microparticles in fetal bovine serum (FBS). 1 g/mL, 1.02 g/mL, 1.05 g/mL, 1.07 g/mL and 1.09 g/mL density microparticles were prepared in fetal bovine serum (FBS) to model patient blood and Pluronic (0.33 %) was added to prevent sticking to the surface of the microfluidic channel. The prepared solutions that contains different Gd (15, 30, 45 and 60 mM) concentrations were loaded into the capillary channel via a pipette and then placed between two magnets. This platform was placed in the bright field microscope system and the capillary channel was monitored with the camera using the 5 × objective.

The linear relationship between the average positions of these microparticles and their density was observed. Thus, by looking at the position of the microparticles inside the capillary channel, density determination can be made (Figure 3.24). According to the position where the microparticle is suspended in FBS, the density was determined.
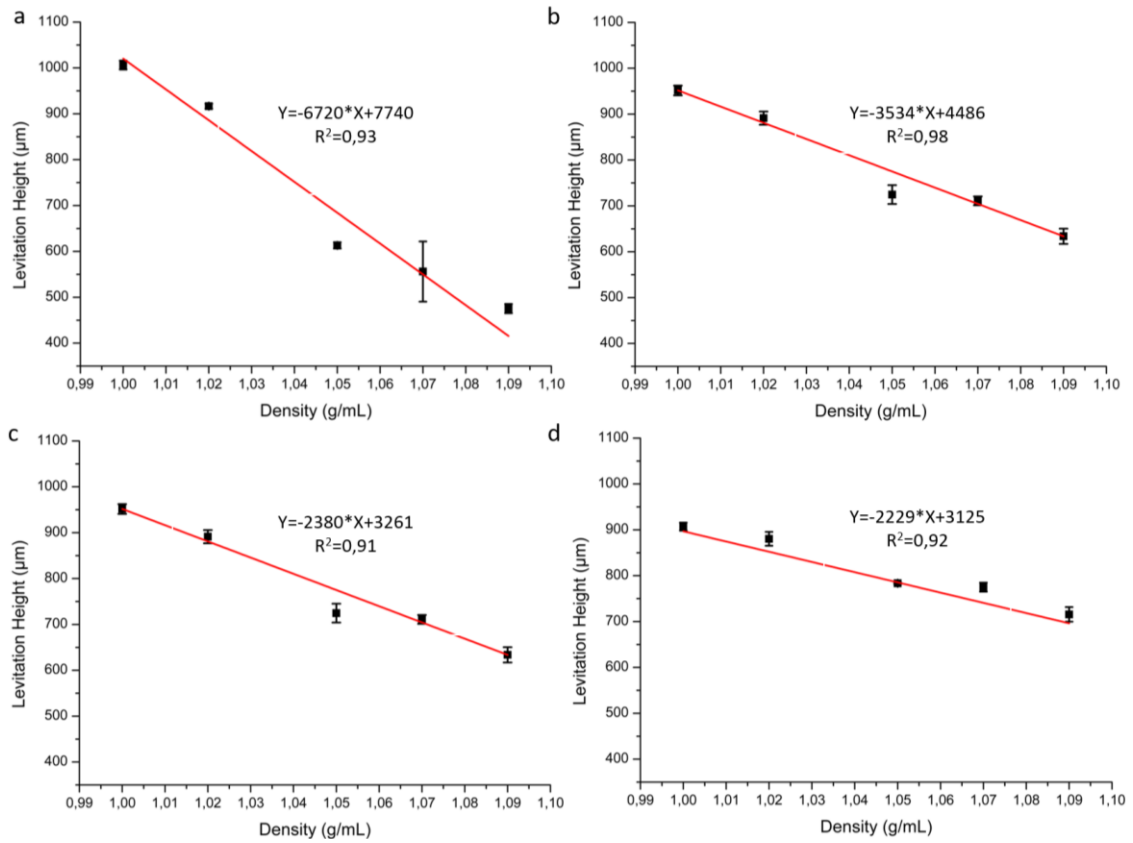
Figure 3.24. Magnetic levitation heights of different density microparticles in FBS. a. in 15 mM, b. in 30 mM, c. in 45 mM and d. in 60 mM Gd concentrations and their linear relations with their densities.

3.7. Determination of The Density of Cells

The magnetic levitation device was used to measure the density of MBA-MB-231 breast cancer cell line and U-937 human monocyte cell line were used in sorting experiments. The cells were prepared in solutions containing 0.33 % Pluronic and 30 mM Gd. The prepared solution was introduced into the capillary channel then placed between two magnets. This platform was placed in the bright field microscope system and the capillary channel was monitored with the camera using the 5 × objective (Figure 3.25).

By using the equation, y=-3534*X+4486 obtained from fig 3.24.b, similar calculations used in the determination of the microparticles densities in PBS were done. The density of MBA-MB-231 was found 1,079 ± 0,002 g/mL whereas for U-937 was 1,094 ± 0,006 g/mL (Figure 3.26).
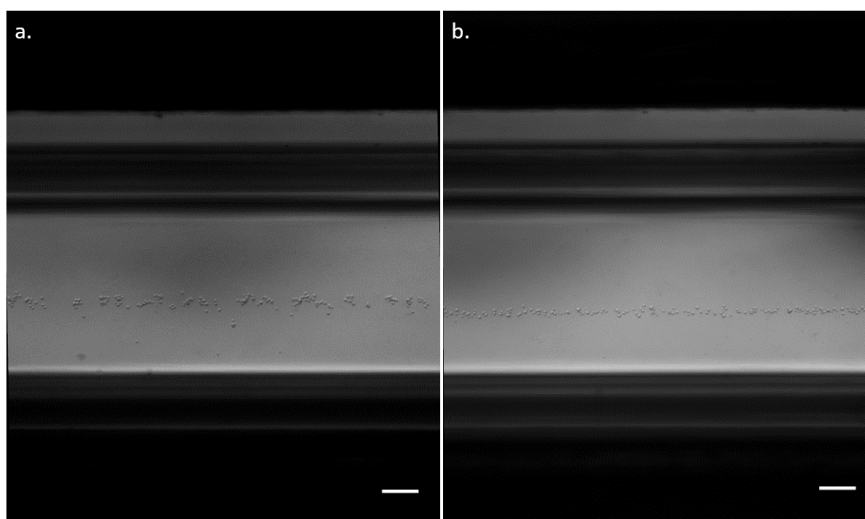
Figure 3.25. Microscopic images of cells in solution containing 30 mM Gd on the magnetic levitation platform. a. The levitation image of MBA-MB-231 breast cancer cell line and b. the levitation image of U-937 human monocyte cell line. The scale bar shows 200 μm.
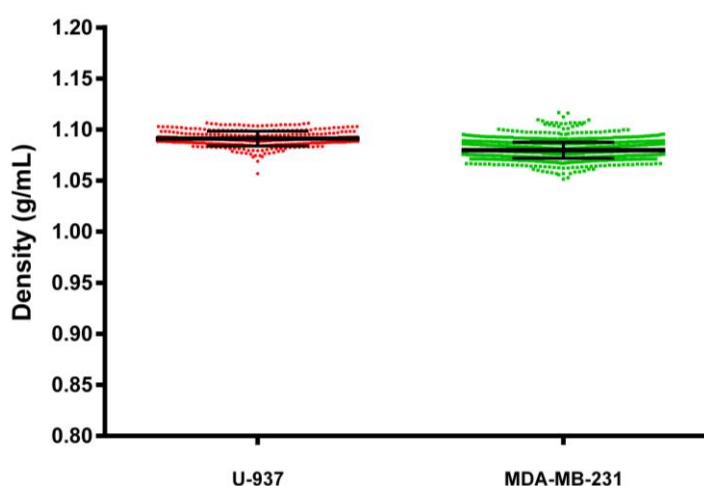
Figure 3.26. The density distribution of cells in 30 mM Gd.

3.8. Sorting of The Microparticles Inside the Microfluidic Channel

The position of the separator in the microfluidic channel (Figure 3.27) used in the sorting experiments corresponds to a levitation height of ~ 650 μm. The separator at this height were used to sort microparticles (or cells) in different density for different Gd concentrations.
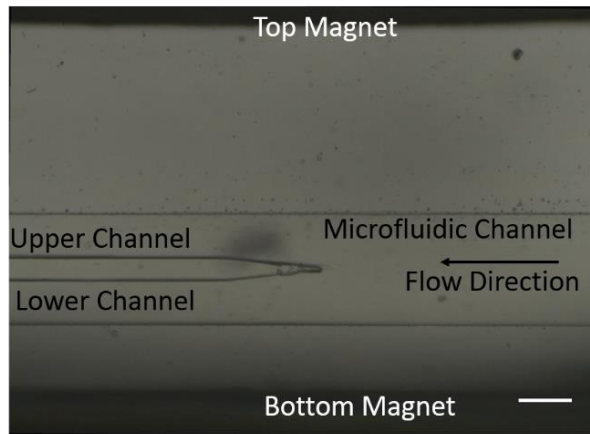
Figure 3.27. Image of the PDMS microfluidic channel used for the sorting processes. The scale bar shows 200 μm.

In other words, when the density-levitation relationship obtained in Figure 3.24 was examined, smaller than 1.05 g/mL density microparticles for 15 mM Gd, 1.07 g mL density particles for 30 mM Gd, 1.10 g/mL density particles for 45 mM Gd and 1.11 g/mL density particles for 60 mM Gd are expected to remain above the separator.

Since the average density of the breast cancer cells in blood was 1.044 g/mL and the average density of the leukocytes was expected to be 1.088 g/mL in blood, when 15 mM-30 mM Gd is used, it is expected that these cells can be separated from each other by staying of blood cells under separator whereas the cancer cells above the separator on the magnetic levitation platform described in Figure 3.28.
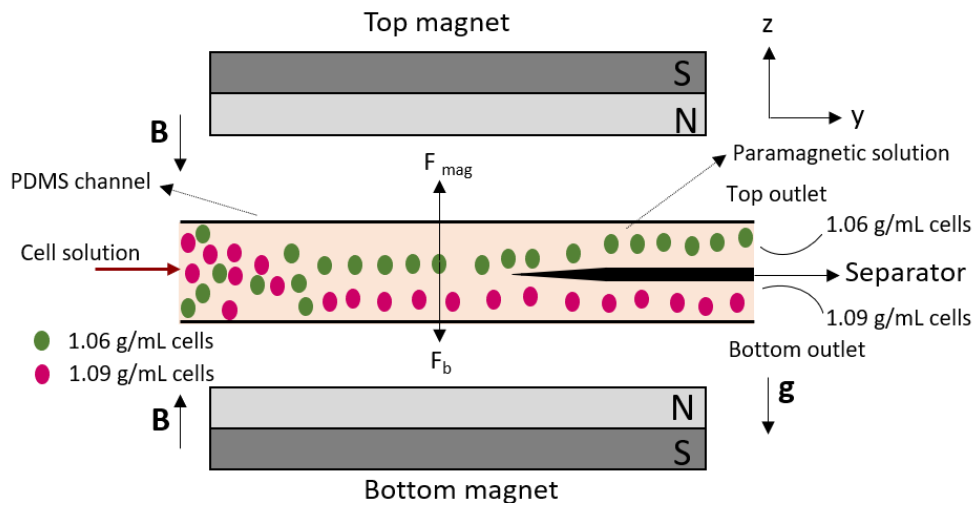
Figure 3.28. Sorting of the cancer cells under flow using the magnetic levitation principle on the microfluidic chip.

Sorting experiments have been carried out to determine the concentration and flow rate of the paramagnetic solution to be used in the microfluidic chip to separate and collect the microparticles efficiently. For this purpose, 1.02 g/mL and 1.09 g/mL microparticles concentrated in 0.33 % Pluronic were injected into the designed microfluidic channel in PBS at a flow rate of 5 µL/min to 20 µL/min with the syringe pump at different (15mM, 30 mM and 60 mM) Gd concentrations (Figure 3.29, Figure 3.30 and Figure 3.31). The separator in the microchannel was located at the middle of the channel (Figure 3.27), so that the microparticles are intended to be directed to the upper or lower channel according to only the levitation heights by ensuring that the hydraulic resistance in the upper and lower channels is equal.

The sorting of the microparticles was observed from the separator region within the microfluidic channel. The sorting efficiency of microparticles was calculated as the ratio of the number of microparticles separated from the top of the separator (upper channel, Figure 3.29, Figure 3.30 and Figure 3.31) to the total number of microparticles collected from outlets.
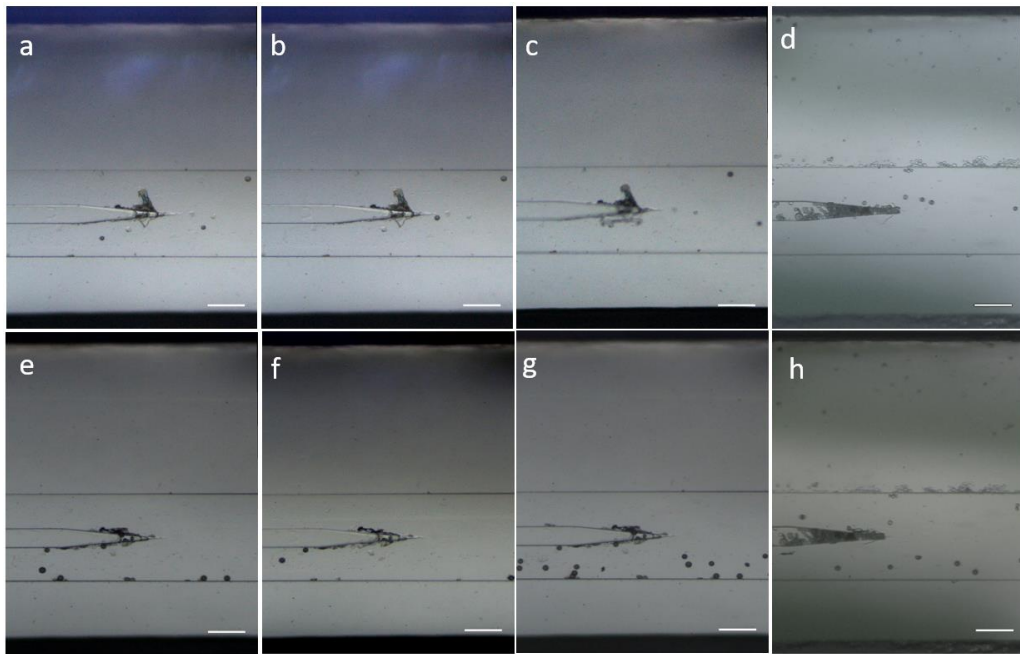
Figure 3.29. Images of 1.02 g/mL and 1.09 g/mL microparticles from the separator part at different flow rates (5-10-15-20 µL/min) in 15 mM Gd. a-d. 1.02 g/mL microparticles under 5 µL/min, 10 µL/min, 15 µL/min and 20 µL/min flow, respectively and e-h. 1.09 g/mL microparticles under 5 µL/min, 10 µL/min, 15 µL/min and 20 µL/min flow, respectively. The scale bar shows 200 µm.

Figure 3.30. Images of 1.02 g/mL and 1.09 g/mL microparticles from the separator part at different flow rates (5-10-15-20 µL/min) in 30 mM Gd. a-d. 1.02 g/mL microparticles under 5 µL/min, 10 µL/min, 15 µL/min and 20 µL/min flow, respectively and e-h. 1.09 g/mL microparticles under 5 µL/min, 10 µL/min, 15 µL/min and 20 µL/min flow, respectively. The scale bar shows 200 µm.

Figure 3.31. Images of 1.02 g/mL and 1.09 g/mL microparticles from the separator part at different flow rates (5-10-15-20 µL/min) in 60 mM Gd. a-d. 1.02 g/mL microparticles under 5 µL/min, 10 µL/min, 15 µL/min and 20 µL/min flow, respectively and e-h. 1.09 g/mL microparticles under 5 µL/min, 10 µL/min, 15 µL/min and 20 µL/min flow, respectively. The scale bar shows 200 µm.

1.02 g/mL density microparticles preferred upper channel with 79.50 % efficiency under 5 µL/min flow, 78.29 % efficiency under 10 µL/min flow, 72.78 % efficiency under 15 µL/min flow and 73.32 % under 20 µL/min flow in 15 mM Gd containing medium. In 30 mM Gd containing medium, they preferred upper channel with 88.47 % efficiency under 5 µL/min flow, 86.74 % efficiency under 10 µL/min flow, 93.11 % efficiency under 15 µL/min flow and 70.54 % efficiency under 20 µL/min flow. In 60 mM Gd containing medium, they preferred upper channel with 93.29 % efficiency under 5 µL/min flow, 83.49 % efficiency under 10 µL/min flow, 80.33 % efficiency under 15 µL/min flow and 86.62 % efficiency under 20 µL/min flow (Figure. 3.32). Even if the 1.02 g/mL microparticles exhibit a large density (0.952-1.100 g/mL) and diameter distribution (9.81-29.43 µm) (Figure 3.22. and 3.23), the microparticles were able to be routed through the upper channel with a separation efficiency of > 90 % under a flow of 15 µL/min in 30 mM Gd.

Figure 3.32. The sorting efficiencies of the microparticles in the upper channel under different flow rates in the media containing different Gadavist concentrations. The sorting efficiencies of a. 1.02 g/mL and b. 1.09 g/mL microparticles in 15 mM, 30 mM and 60 mM Gd.

1.09 g/mL density microparticles preferred bottom channel with 8.71 % efficiency under 5 µL/min flow, 10.32 % efficiency under 10 µL/min flow, 8.54 % efficiency under 15 µL/min flow and 6.04 % under 20 µL/min flow in 15 mM Gd containing medium. In 30 mM Gd containing medium, they preferred bottom channel with 8.54 % efficiency under 5 µL/min flow, 5.39 % efficiency under 10 µL/min flow, 14.13 % efficiency under 15 µL/min flow and 10.21 % efficiency under 20 µL/min flow. In 60 mM Gd containing medium, they preferred bottom channel with 18.62 % efficiency under 5 µL/min flow,

27.46 % efficiency under 10 µL/min flow, 14.77 % efficiency under 15 µL/min flow and 17.82 % efficiency under 20 µL/min flow (Figure 3.32). Not surprisingly, even if 1.09 g/mL microparticles present a large density distribution (0.975-1.411 g/mL), most of these particles preferred the bottom channel at different flow rates and Gd concentrations.

Microparticles were prepared in fetal bovine serum (FBS) to model patient blood and Pluronic (0.33 %) was added to prevent sticking to the surface of the microfluidic channel. The prepared microparticles were given to the microfluidic channel at different flow rates (5-10-15-20 µL/min) in the medium containing 30 mM Gd (Figure 3.33) and the sorting efficiency according to the upper channel was analyzed.
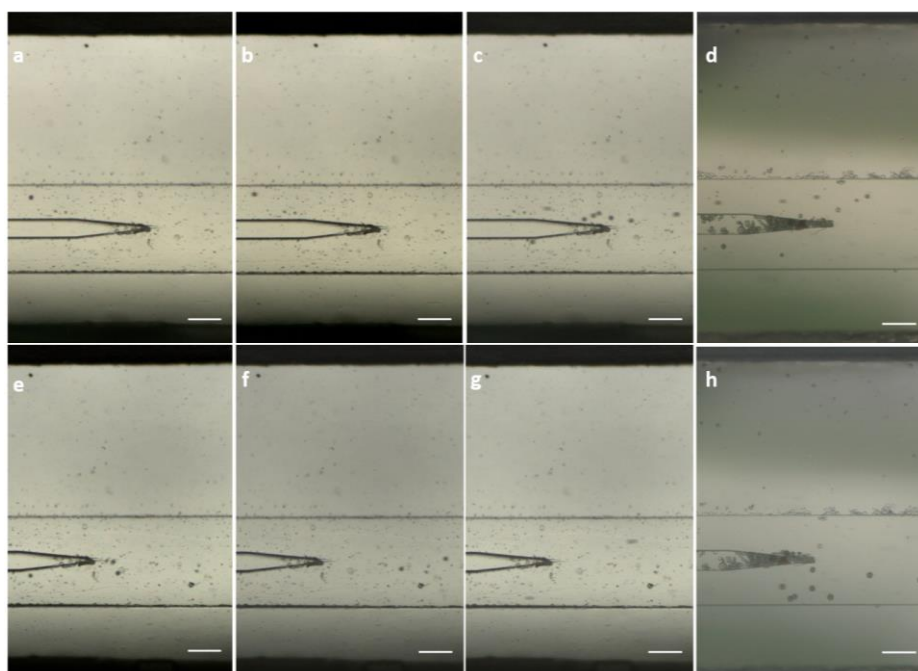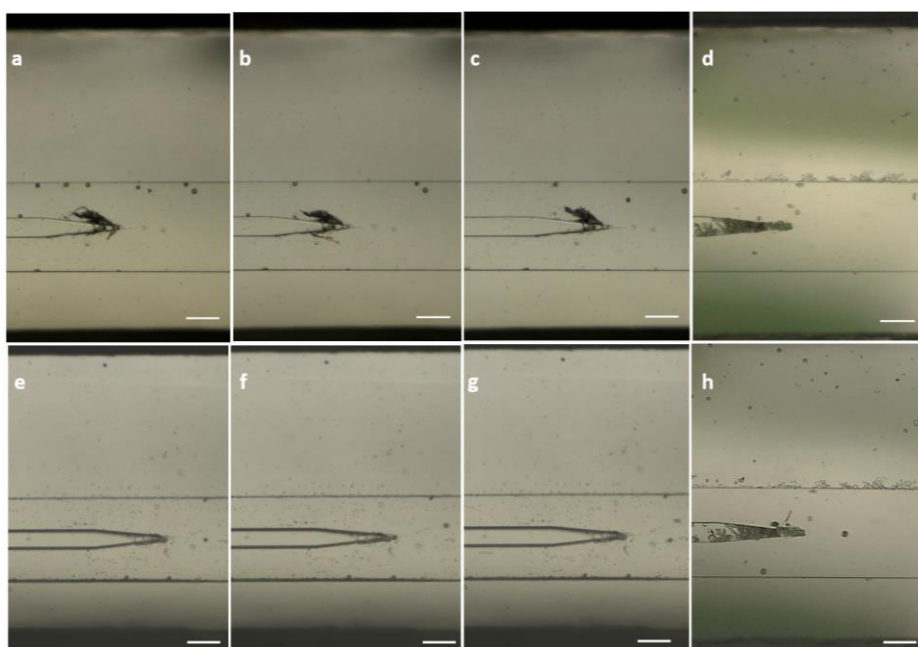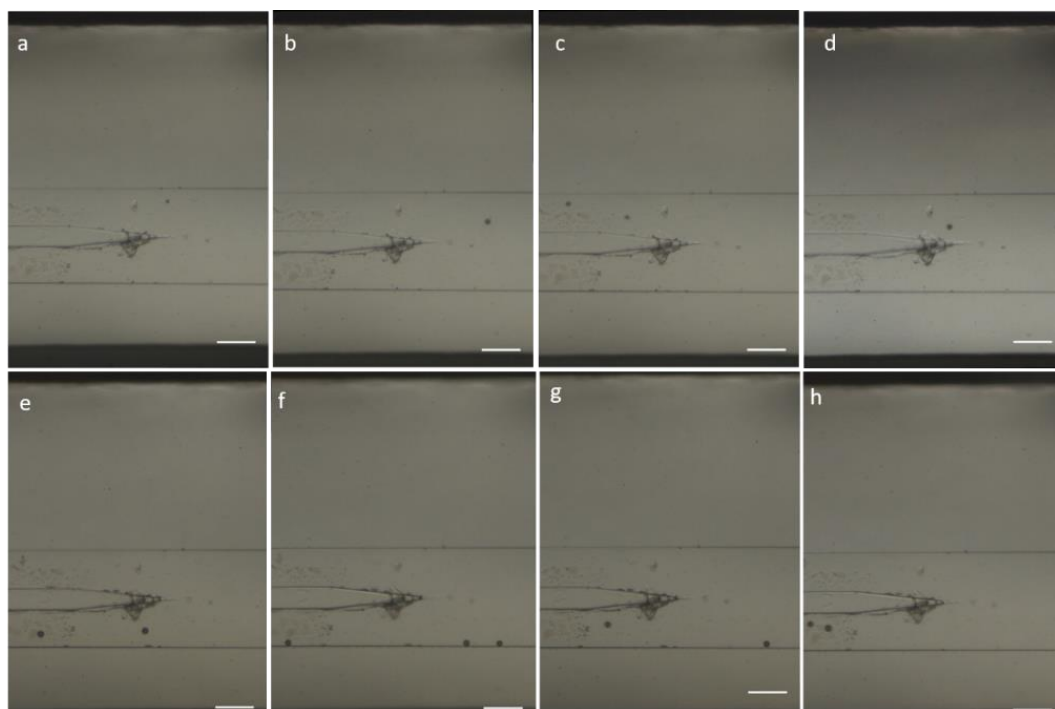

Figure 3.33. Images of 1.02 g/mL and 1.09 g/mL microparticles from the separator part at different flow rates (5-10-15-20 µL/min) in medium containing 30mM Gd and FBS. a-d. 1.02 g/mL microparticles under 5 µL/min, 10 µL/min, 15 µL/min and 20 µL/min flow, respectively and e-h. 1.09 g/mL microparticles under 5 µL/min, 10 µL/min, 15 µL/min and 20 µL/min flow, respectively. The scale bar shows 200 µm.

1.02 g/mL density microparticles preferred upper channel with 90.17 % efficiency under 5 µL/min flow, 86.22 % efficiency under 10 µL/min flow, 89.43 % efficiency under 15 µL/min flow and 74.55 % under 20 µL/min flow in 30 mM Gd and FBS (Figure 3.34.a).
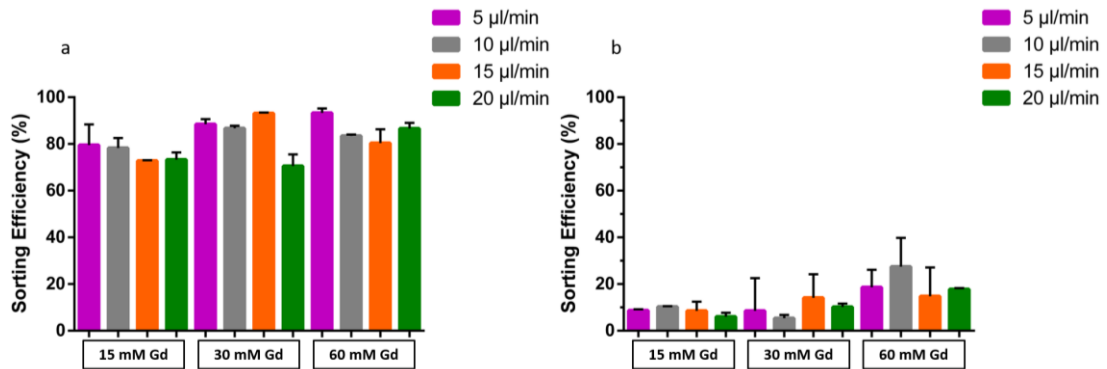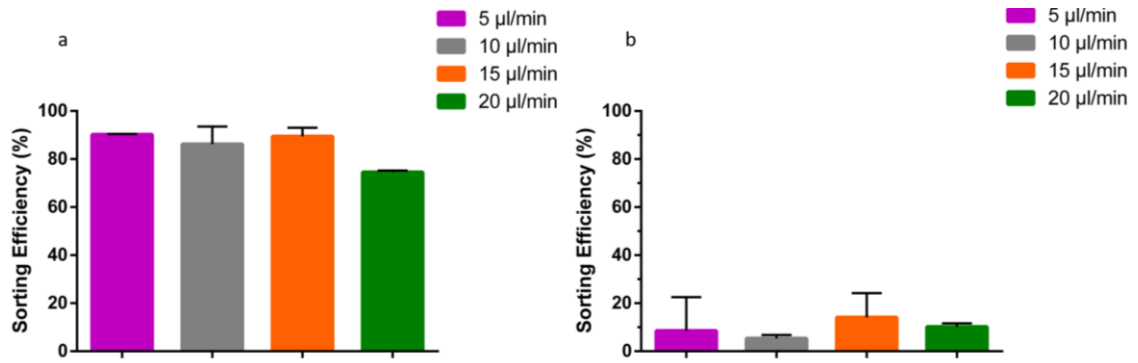
Figure 3.34. The sorting efficiencies of the microparticles in the upper channel under different flow rates in the media containing 30 mM Gd and FBS. The sorting efficiencies of a. 1.02 g/mL and b. 1.09 g/mL microparticles.

On the other side, 1.09 g/mL density microparticles preferred upper channel with 9.88 % efficiency under 5 µL/min flow, 4.44 % efficiency under 10 µL/min flow, 4.08 % efficiency under 15 µL/min flow and 11.53 % under 20 µL/min flow in 30 mM Gd and FBS (Figure 3.34.b).

The results of the experiments show that ~ 90 % of the 1.02 g/mL microparticles and 5 % of the 1.09 g/mL microparticles at 15 µL /min flow were sorted from the upper channel in FBS. This shows that 90 % sorting and efficiency of the study objectives have been achieved. At the same time, the flow rate is very close to the desired (1 mL/h rate). In addition, the sorting experiments that perform in PBS and FBS have been finalized with similar results.

3.9. Sorting of The Cells Inside the Microfluidic Channel

The number of CTCs in the human whole blood are found with a concentration of 1−100 cells/mL, which also contains great numbers of leukocytes (~4 x10^6/mL) [95, 96]. To model the human blood, three different cell concentrations of U-937 human monocyte cells (10^7 cells/mL, 10^6 cells/mL and 10^5 cells/mL) and MBA-MB-231 breast cancer cells (10^3 cells/mL, 10^2 cells/mL and 10 cells/mL) were sorted in different Gd concentrations to find the optimum and high efficiency under 1 mL/h flow rate.

U-937 human monocyte cells at 10^7 cells/mL concentration preferred upper channel with 8.47 % efficiency, at 10^6 cells/mL with 7.30 % efficiency, at 10^5 cells/mL with % 9.15 efficiency, under 1 mL/h flow in 20 mM Gd. In 30mM Gd, cells at 10^7 cells/mL concentration preferred upper channel with 2.17 % efficiency, at 10^6 cells/mL with % 9.50 efficiency and 10^5 cells/mL with % 13.20 efficiency under 1 mL/h flow. In 40 mM Gd containing medium, cells at 10^7 cells/mL concentration preferred upper channel with 20.00 % efficiency, at 10^6 cells/mL with % 6.05 efficiency and 10^5 cells/mL with % 15.72 efficiency under 1 mL/h flow (Figure 3.35).
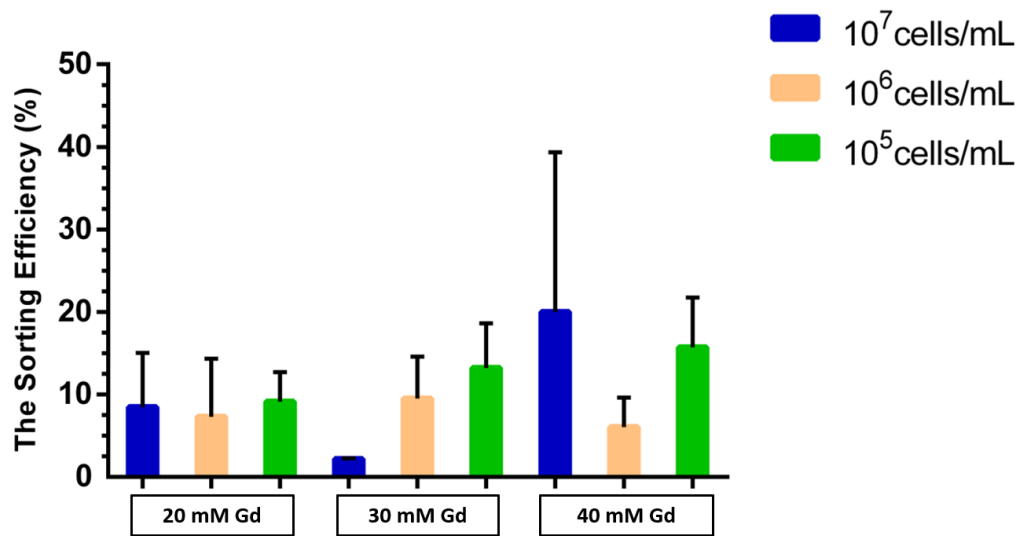
Figure 3.35. The sorting efficiencies of U-937 cell line in different concentrations (10^5 cells/mL, 10^6 cells/mL and 10^7 cells/mL) in the upper channel under 1 mL/h flow rate in the media containing 20 mM, 30 mM and 40 mM Gadavist.

MBA-MB-231 breast cancer cells at 10^3 cells/mL concentration preferred upper channel with 54.41 % efficiency, at 10^2 cells/mL with 47.44 % efficiency and 10 cells/mL with 44.44 % efficiency, under 1 mL/h flow in 20 mM Gd. In 30mM Gd, cells at 10^3 cells/mL concentration preferred upper channel with 88.38 % efficiency, at 10^2 cells/mL with % 83.83 efficiency and 10 cells/mL with % 66.75 efficiency under 1 mL/h flow. Moreover, in 40 mM Gd containing medium, cells at 10^3 cells/mL concentration preferred upper channel with 83.37 % efficiency, at 10^2 cells/mL with % 86.40 efficiency and 10 cells/mL with % 87.67 efficiency under 1 mL/h flow (Figure 3.36).
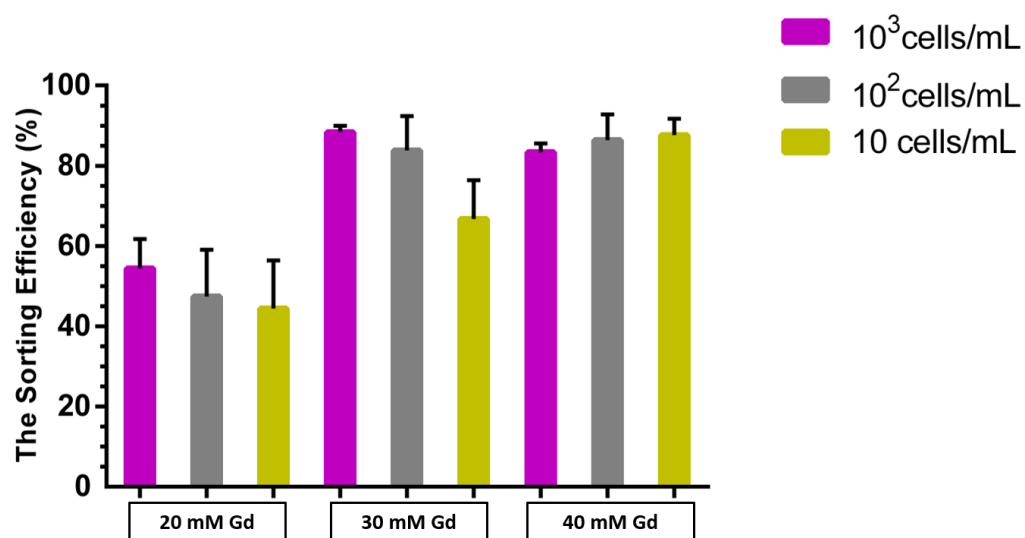
Figure 3.36. The sorting efficiencies of MDA-MB-231 cell line in different concentrations (10 cells/mL, 10^2 cells/mL and 10^3 cells/mL) in the upper channel under 1 mL/h flow rate in the media containing 20 mM, 30 mM and 40 mM Gadavist.

CHAPTER 4

CONCLUSION

Cancer metastasis is the major cause (more than 90 %) of cancer related death. Feasible tumor cells frequently change their genetic and biological forms that can invade blood vessels and migrate around the body as circulating tumor cells (CTCs). Therefore, there is no standard property or parameter that separates CTCs from blood cells.

The currently available technology in the market considered as the state of the art, CellSearch ® has relied on immunomagnetic sorting. It sorts CTCs from 60 % of metastatic patients and about 30 % of non-metastatic patients.

Despite all challenging characteristics of tumor cells, many clinical studies and an increase in recovery rate from the disease, inversely related to the number of CTCs in the blood, have revealed the importance of investigation and sorting of tumor cells. The magnetic levitation principle has the potential to overcome all limitations by detecting a small number of CTCs within the blood cells. The platform that works with the magnetic forces can be presented as a novel, more reliable, less risky, less complex (i.e. biopsy) and cost-effective (fabrication with 3D printer) technology for the early diagnosis of cancer compared to existing methods (i.e. FACS and MACS).

The developed magnetic levitation platform has higher sorting efficiency (in 30 mM Gadavist for 10^3 cells/mL is 88.38 % , for 10^2 cells/mL 83.83 %, for 10 cells/mL 66.75 % and in 40 mM Gadavist for 10^3 cells/mL is 83.37 %, for 10^2 cells/mL 86.40 %, for 10 cells/mL 87.67 %) of breast cancer cells (MDA-MB-231) than CellSearch system (28.3 % from nonmetastatic patient's blood). However, due to the low abundance of CTCs in human blood, the low concentration of breast cancer cells (~ 10 /mL) should be sorted more efficiently means more than 90 %. This was achieved by increasing the Gadavist concentration from 30 mM to 40 mM, dependently the sorting efficiency of U-937 human monocyte cells.

Additionally, U-937 cells at 10^7 cells/mL concentration preferred the upper channel with 8.47 % efficiency, at 10^6 cells/mL with 7.30 % efficiency and at 10^5 cells/mL with % 9.15 efficiency, under 1 mL/h flow in 20 mM Gd. In 30mM Gd, cells at

10^7 cells/mL concentration preferred upper channel with 2.17 % efficiency, at 10^6 cells/mL with % 9.50 efficiency and 10^5 cells/mL with % 13.20 efficiency under 1 mL/h flow. In 40 mM Gd containing medium, cells at 10^7 cells/mL concentration preferred upper channel with 20.00 % efficiency, at 10^6 cells/mL with % 6.05 efficiency and 10^5 cells/mL with % 15.72 efficiency under 1 mL/h flow. According to the presented results for the next experiments include sorting of mixed MDA-MB-231 and U-937 cells, the optimum Gadavist and cell concentration was decided as 10^2 MDA-MB-231 cells/mL and 10^7 U-937 cells/mL in 30 Mm Gd while achieving higher sorting efficiency for both.

As a result of this master study, cancer cells have been sorted for the first time on the microfluidic chip based on their densities. Thus, cancer cells can be more easily separated from white blood cells by applying very sensitive forces to them. The developed magnetic levitation platform can be used for rapid, low cost and label-free in-vitro diagnosis of cancer by sorting CTCs from whole blood in a high-throughput manner. The sorted cells might further be collected for downstream analysis for personalized medicine.

REFERENCES

1.   Shen, Y.; Yalikun, Y.; Tanaka, Y., Recent advances in microfluidic cell sorting systems. *Sensors and Actuators B: Chemical* **2019,** *282*, 268-281.

2.   Shields, C. W. t.; Reyes, C. D.; Lopez, G. P., Microfluidic cell sorting: a review of the advances in the separation of cells from debulking to rare cell isolation. *Lab Chip* **2015,** *15* (5), 1230-49.

3.   Carey, T. R.; Cotner, K. L.; Li, B.; Sohn, L. L., Developments in label-free microfluidic methods for single-cell analysis and sorting. *Wiley Interdiscip Rev Nanomed Nanobiotechnol* **2019,** *11* (1), e1529.

4.   Yaman, S.; Anil-Inevi, M.; Ozcivici, E.; Tekin, H. C., Magnetic Force-Based Microfluidic Techniques for Cellular and Tissue Bioengineering. *Front Bioeng Biotechnol* **2018,** *6*, 192.

5.   Horak, D.; Svobodova, Z.; Autebert, J.; Coudert, B.; Plichta, Z.; Kralovec, K.; Bilkova, Z.; Viovy, J. L., Albumin-coated monodisperse magnetic poly(glycidyl methacrylate) microspheres with immobilized antibodies: application to the capture of epithelial cancer cells. *J Biomed Mater Res A* **2013,** *101* (1), 23-32.

6.   Jarvas, G.; Guttman, A., Modeling of cell sorting and rare cell capture with microfabricated biodevices. *Trends Biotechnol* **2013,** *31* (12), 696-703.

7.   Saias, L.; Saliba, A.-E.; Viovy, J.-L.; Pierga, J.-Y.; Vielh, P.; Farace, F., Microfluidic magnetic cell sorting system for cancer diagnosis. *La Houille Blanche* **2009,** (5), 105-111.

8.   Chen, J.; Li, J.; Sun, Y., Microfluidic approaches for cancer cell detection, characterization, and separation. *Lab Chip* **2012,** *12* (10), 1753-67.

9.   Besant, J. D.; Mohamadi, R. M.; Aldridge, P. M.; Li, Y.; Sargent, E. H.; Kelley, S. O., Velocity valleys enable efficient capture and spatial sorting of nanoparticle-bound cancer cells. *Nanoscale* **2015,** *7* (14), 6278-85.

10.   Kim, M.; Mo Jung, S.; Lee, K. H.; Jun Kang, Y.; Yang, S., A microfluidic device for continuous white blood cell separation and lysis from whole blood. *Artif Organs* **2010,** *34* (11), 996-1002.

11.   Herzenberg, L. A.; Sweet, R. G.; Herzenberg, L. A., Fluorescence-activated cell sorting. *Scientific American* **1976,** *234* (3), 108-118.

12.   Herzenberg, L. A.; Parks, D.; Sahaf, B.; Perez, O.; Roederer, M.; Herzenberg, L. A., The History and Future of the Fluorescence Activated Cell Sorter and Flow Cytometry: A View from Stanford. *Clinical Chemistry* **2002,** *48* (10), 1819-1827.

13.   Hulett, H. R.; Bonner, W. A.; Barrett, J.; Herzenberg, L. A., Cell sorting: automated separation of mammalian cells as a function of intracellular fluorescence. *Science (New York, N.Y.)* **1969,** *166* (3906), 747-9.

14.   Hu, P.; Zhang, W.; Xin, H.; Deng, G., Single Cell Isolation and Analysis. *Front Cell Dev Biol* **2016,** *4*, 116.

15.   Hodne, K.; Weltzien, F. A., Single-Cell Isolation and Gene Analysis: Pitfalls and Possibilities. *Int J Mol Sci* **2015,** *16* (11), 26832-49.

16.   Gross, A.; Schoendube, J.; Zimmermann, S.; Steeb, M.; Zengerle, R.; Koltay, P., Technologies for Single-Cell Isolation. *Int J Mol Sci* **2015,** *16* (8), 16897-919.

17.   Yousuff, C.; Ho, E.; Hussain K, I.; Hamid, N., Microfluidic Platform for Cell Isolation and Manipulation Based on Cell Properties. *Micromachines* **2017,** *8* (1).

18.   Piyasena, M. E.; Graves, S. W., The intersection of flow cytometry with microfluidics and microfabrication. *Lab Chip* **2014,** *14* (6), 1044-59.

19.   Hosic, S.; Murthy, S. K.; Koppes, A. N., Microfluidic Sample Preparation for Single Cell Analysis. *Anal Chem* **2016,** *88* (1), 354-80.

20.   Picot, J.; Guerin, C. L.; Le Van Kim, C.; Boulanger, C. M., Flow cytometry: retrospective, fundamentals and recent instrumentation. *Cytotechnology* **2012,** *64* (2), 109-30.

21. Rana, A.; Zhang, Y.; Esfandiari, L., Advancements in microfluidic technologies for isolation and early detection of circulating cancer-related biomarkers. *Analyst* **2018,** *143* (13), 2971-2991.

22. Pamme, N.; Wilhelm, C., Continuous sorting of magnetic cells via on-chip free-flow magnetophoresis. *Lab Chip* **2006,** *6* (8), 974-80.

23. Bednarz-Knoll, N.; Efstathiou, A.; Gotzhein, F.; Wikman, H.; Mueller, V.; Kang, Y.; Pantel, K., Potential Involvement of Jagged1 in Metastatic Progression of Human Breast Carcinomas. *Clin Chem* **2016,** *62* (2), 378-86.

24. Fernandez-Carrascal, A.; Garcia-Algar, M.; Nazarenus, M.; Torres-Nuñez, A.; Guerrini, L.; Feliu, N.; Parak, W. J.; Garcia-Rico, E.; Alvarez-Puebla, R. A., Metabolic pathway for the universal fluorescent recognition of tumor cells. *Oncotarget* **2017,** *8* (44), 76108-76115.

25. Fizazi, K.; Morat, L.; Chauveinc, L.; Prapotnich, D.; De Crevoisier, R.; Escudier, B.; Cathelineau, X.; Rozet, F.; Vallancien, G.; Sabatier, L.; Soria, J. C., High detection rate of circulating tumor cells in blood of patients with prostate cancer using telomerase activity. *Ann Oncol* **2007,** *18* (3), 518-21.

26. Stefansson, S.; Adams, D. L.; Ershler, W. B.; Le, H.; Ho, D. H., A cell transportation solution that preserves live circulating tumor cells in patient blood samples. *BMC Cancer* **2016,** *16*, 300.

27. Zhang, X.; Hofmann, S.; Rack, B.; Harbeck, N.; Jeschke, U.; Sixou, S., Fluorescence Analysis of Vitamin D Receptor Status of Circulating Tumor Cells (CTCS) in Breast Cancer: From Cell Models to Metastatic Patients. *Int J Mol Sci* **2017,** *18* (6).

28. Zhu, P.; Stanton, M. L.; Castle, E. P.; Joseph, R. W.; Adams, D. L.; Li, S.; Amstutz, P.; Tang, C. M.; Ho, T. H., Detection of tumor-associated cells in cryopreserved peripheral blood mononuclear cell samples for retrospective analysis. *J Transl Med* **2016,** *14* (1), 198.

29. Cho, H.; Kim, J.; Song, H.; Sohn, K. Y.; Jeon, M.; Han, K. H., Microfluidic technologies for circulating tumor cell isolation. *Analyst* **2018,** *143* (13), 2936-2970.

30. Kallergi, G.; Politaki, E.; Alkahtani, S.; Stournaras, C.; Georgoulias, V., Evaluation of Isolation Methods for Circulating Tumor Cells (CTCs). *Cell Physiol Biochem* **2016,** *40* (3-4), 411-419.

31. Anil-Inevi, M.; Yilmaz, E.; Sarigil, O.; Tekin, H. C.; Ozcivici, E., Single Cell Densitometry and Weightlessness Culture of Mesenchymal Stem Cells Using Magnetic Levitation. *Methods Mol Biol* **2019**.

32. Sarigil, O.; Anil-Inevi, M.; Yilmaz, E.; Mese, G.; Tekin, H. C.; Ozcivici, E., Label-free density-based detection of adipocytes of bone marrow origin using magnetic levitation. *Analyst* **2019,** *144* (9), 2942-2953.

33. Bryan, A. K.; Hecht, V. C.; Shen, W.; Payer, K.; Grover, W. H.; Manalis, S. R., Measuring single cell mass, volume, and density with dual suspended microchannel resonators. *Lab Chip* **2014,** *14* (3), 569-576.

34. Zhao, Y.; Lai, H. S.; Zhang, G.; Lee, G. B.; Li, W. J., Rapid determination of cell mass and density using digitally controlled electric field in a microfluidic chip. *Lab Chip* **2014,** *14* (22), 4426-34.

35. Reyes, D. R.; Iossifidis, D.; Auroux, P.-A.; Manz, A., Micro Total Analysis Systems. 1. Introduction, Theory, and Technology. *Analytical Chemistry* **2002,** *74* (12), 2623-2636.

36. Hejazian, M.; Li, W.; Nguyen, N. T., Lab on a chip for continuous-flow magnetic cell separation. *Lab Chip* **2015,** *15* (4), 959-70.

37. Gijs, M. A.; Lacharme, F.; Lehmann, U., Microfluidic applications of magnetic particles for biological analysis and catalysis. *Chemical reviews* **2010,** *110* (3), 1518-63.

38. Gregoratto, I.; McNeil, C. J.; Reeks, M. W., Micro-devices for rapid continuous separation of suspensions for use in micro-total-analysis-systems (μTAS). In *Microfluidics, BioMEMS, and Medical Microsystems V*, 2007.

39. Lisowski, P.; Zarzycki, P. K., Microfluidic Paper-Based Analytical Devices (muPADs) and Micro Total Analysis Systems (muTAS): Development, Applications and Future Trends. *Chromatographia* **2013,** *76*, 1201-1214.

40.   Vilkner, T.; Janasek, D.; Manz, A., Micro Total Analysis Systems. Recent Developments. *Analytical Chemistry* **2004,** *76* (12), 3373-3386.

41.   West, J.; Becker, M.; Tombrink, S.; Manz, A., Micro Total Analysis Systems: Latest Achievements. *Analytical Chemistry* **2008,** *80* (12), 4403-4419.

42.   Chudziak, J.; Burt, D. J.; Mohan, S.; Rothwell, D. G.; Mesquita, B.; Antonello, J.; Dalby, S.; Ayub, M.; Priest, L.; Carter, L.; Krebs, M. G.; Blackhall, F.; Dive, C.; Brady, G., Clinical evaluation of a novel microfluidic device for epitope-independent enrichment of circulating tumour cells in patients with small cell lung cancer. *Analyst* **2016,** *141* (2), 669-78.

43.   Fan, X.; Jia, C.; Yang, J.; Li, G.; Mao, H.; Jin, Q.; Zhao, J., A microfluidic chip integrated with a high-density PDMS-based microfiltration membrane for rapid isolation and detection of circulating tumor cells. *Biosens Bioelectron* **2015,** *71*, 380-386.

44.   Tang, Y.; Shi, J.; Li, S.; Wang, L.; Cayre, Y. E.; Chen, Y., Microfluidic device with integrated microfilter of conical-shaped holes for high efficiency and high purity capture of circulating tumor cells. *Sci Rep* **2014,** *4*, 6052.

45.   Bhagat, A. A. S.; Kuntaegowdanahalli, S. S.; Papautsky, I., Enhanced particle filtration in straight microchannels using shear-modulated inertial migration. *Physics of Fluids* **2008,** *20* (10), 101702.

46.   Zhou, J.; Giridhar, P. V.; Kasper, S.; Papautsky, I., Modulation of rotation-induced lift force for cell filtration in a low aspect ratio microchannel. *Biomicrofluidics* **2014,** *8* (4), 044112-044112.

47.   Che, J.; Yu, V.; Dhar, M.; Renier, C.; Matsumoto, M.; Heirich, K.; Garon, E. B.; Goldman, J.; Rao, J.; Sledge, G. W.; Pegram, M. D.; Sheth, S.; Jeffrey, S. S.; Kulkarni, R. P.; Sollier, E.; Di Carlo, D., Classification of large circulating tumor cells isolated with ultra-high throughput microfluidic Vortex technology. *Oncotarget* **2016,** *7* (11), 12748-60.

48.   Ozkumur, E.; Shah, A. M.; Ciciliano, J. C.; Emmink, B. L.; Miyamoto, D. T.; Brachtel, E.; Yu, M.; Chen, P.-i.; Morgan, B.; Trautwein, J.; Kimura, A.; Sengupta, S.; Stott, S. L.; Karabacak, N. M.; Barber, T. A.; Walsh, J. R.; Smith, K.; Spuhler, P. S.; Sullivan, J. P.; Lee, R. J.; Ting, D. T.; Luo, X.; Shaw, A. T.; Bardia, A.; Sequist, L. V.; Louis, D. N.; Maheswaran, S.; Kapur, R.; Haber, D. A.; Toner, M., Inertial focusing for tumor antigen-

dependent and -independent sorting of rare circulating tumor cells. *Sci Transl Med* **2013,** *5* (179), 179ra47-179ra47.

49.   Loutherback, K.; D'Silva, J.; Liu, L.; Wu, A.; Austin, R. H.; Sturm, J. C., Deterministic separation of cancer cells from blood at 10 mL/min. *AIP Adv* **2012,** *2* (4), 42107.

50.   Hur, S. C.; Mach, A. J.; Di Carlo, D., High-throughput size-based rare cell enrichment using microscale vortices. *Biomicrofluidics* **2011,** *5* (2), 22206.

51.   Abdulla, A.; Liu, W.; Gholamipour-Shirazi, A.; Sun, J.; Ding, X., High-Throughput Isolation of Circulating Tumor Cells Using Cascaded Inertial Focusing Microfluidic Channel. *Anal Chem* **2018,** *90* (7), 4397-4405.

52.   Huang, L. R.; Cox, E. C.; Austin, R. H.; Sturm, J. C., Continuous particle separation through deterministic lateral displacement. *Science (New York, N.Y.)* **2004,** *304* (5673), 987-90.

53.   Bhagat, A. A.; Bow, H.; Hou, H. W.; Tan, S. J.; Han, J.; Lim, C. T., Microfluidics for cell separation. *Med Biol Eng Comput* **2010,** *48* (10), 999-1014.

54.   Chen, Y.; Li, P.; Huang, P. H.; Xie, Y.; Mai, J. D.; Wang, L.; Nguyen, N. T.; Huang, T. J., Rare cell isolation and analysis in microfluidics. *Lab Chip* **2014,** *14* (4), 626-45.

55.   Liu, Z.; Huang, F.; Du, J.; Shu, W.; Feng, H.; Xu, X.; Chen, Y., Rapid isolation of cancer cells using microfluidic deterministic lateral displacement structure. *Biomicrofluidics* **2013,** *7* (1), 11801.

56.   Low, W. S.; Wan Abas, W. A., Benchtop technologies for circulating tumor cells separation based on biophysical properties. *Biomed Res Int* **2015,** *2015*, 239362.

57.   Lee, A.; Park, J.; Lim, M.; Sunkara, V.; Kim, S. Y.; Kim, G. H.; Kim, M. H.; Cho, Y. K., All-in-one centrifugal microfluidic device for size-selective circulating tumor cell isolation with high purity. *Anal Chem* **2014,** *86* (22), 11349-56.

58.   Song, J.; Song, M.; Kang, T.; Kim, D.; Lee, L. P., Label-free density difference amplification-based cell sorting. *Biomicrofluidics* **2014,** *8* (6), 064108.

59.   Büyükkoçak, S.; Özer, M. B.; Çetin, B., Numerical modeling of ultrasonic particle manipulation for microfluidic applications. *Microfluidics and Nanofluidics* **2014,** *17* (6), 1025-1037.

60.   Magnusson, C.; Augustsson, P.; Lenshof, A.; Ceder, Y.; Laurell, T.; Lilja, H., Clinical-Scale Cell-Surface-Marker Independent Acoustic Microfluidic Enrichment of Tumor Cells from Blood. *Anal Chem* **2017,** *89* (22), 11954-11961.

61.   Cushing, K.; Undvall, E.; Ceder, Y.; Lilja, H.; Laurell, T., Reducing WBC background in cancer cell separation products by negative acoustic contrast particle immuno-acoustophoresis. *Anal Chim Acta* **2018,** *1000*, 256-264.

62.   Lee, G.-H.; Kim, S.-H.; Ahn, K.; Lee, S.-H.; Park, J. Y., Separation and sorting of cells in microsystems using physical principles. *Journal of Micromechanics and Microengineering* **2016,** *26* (1).

63.   Moon, H. S.; Kwon, K.; Kim, S. I.; Han, H.; Sohn, J.; Lee, S.; Jung, H. I., Continuous separation of breast cancer cells from blood samples using multi-orifice flow fractionation (MOFF) and dielectrophoresis (DEP). *Lab Chip* **2011,** *11* (6), 1118-25.

64.   Huang, S. B.; Wu, M. H.; Lin, Y. H.; Hsieh, C. H.; Yang, C. L.; Lin, H. C.; Tseng, C. P.; Lee, G. B., High-purity and label-free isolation of circulating tumor cells (CTCs) in a microfluidic platform by using optically-induced-dielectrophoretic (ODEP) force. *Lab Chip* **2013,** *13* (7), 1371-83.

65.   Furlani, E. P., Magnetophoretic separation of blood cells at the microscale. *Journal of Physics D: Applied Physics* **2007,** *40* (5), 1313-1319.

66.   Inglis, D. W.; Riehn, R.; Sturm, J. C.; Austin, R. H., Microfluidic high gradient magnetic cell separation. *Journal of Applied Physics* **2006,** *99* (8).

67.   Nam, J.; Huang, H.; Lim, H.; Lim, C.; Shin, S., Magnetic separation of malaria-infected red blood cells in various developmental stages. *Anal Chem* **2013,** *85* (15), 7316-23.

68.   Shen, F.; Hwang, H.; Hahn, Y. K.; Park, J. K., Label-free cell separation using a tunable magnetophoretic repulsion force. *Anal Chem* **2012,** *84* (7), 3075-81.

69.   Trzpis, M.; McLaughlin, P. M.; de Leij, L. M.; Harmsen, M. C., Epithelial cell adhesion molecule: more than a carcinoma marker and adhesion molecule. *Am J Pathol* **2007,** *171* (2), 386-95.

70.   Liao, M. Y.; Lai, J. K.; Kuo, M. Y.; Lu, R. M.; Lin, C. W.; Cheng, P. C.; Liang, K. H.; Wu, H. C., An anti-EpCAM antibody EpAb2-6 for the treatment of colon cancer. *Oncotarget* **2015,** *6* (28), 24947-68.

71.   Kwak, B.; Lee, J.; Lee, J.; Kim, H. S.; Kang, S.; Lee, Y., Spiral shape microfluidic channel for selective isolating of heterogenic circulating tumor cells. *Biosens Bioelectron* **2018,** *101*, 311-316.

72.   Kwak, B.; Lee, J.; Lee, D.; Lee, K.; Kwon, O.; Kang, S.; Kim, Y., Selective isolation of magnetic nanoparticle-mediated heterogeneity subpopulation of circulating tumor cells using magnetic gradient based microfluidic system. *Biosens Bioelectron* **2017,** *88*, 153-158.

73.   Wang, X.; Sun, L.; Zhang, H.; Wei, L.; Qu, W.; Zeng, Z.; Liu, Y.; Zhu, Z., Microfluidic chip combined with magnetic-activated cell sorting technology for tumor antigen-independent sorting of circulating hepatocellular carcinoma cells. *PeerJ* **2019,** *7*, e6681.

74.   Durmus, N. G.; Tekin, H. C.; Guven, S.; Sridhar, K.; Arslan Yildiz, A.; Calibasi, G.; Ghiran, I.; Davis, R. W.; Steinmetz, L. M.; Demirci, U., Magnetic levitation of single cells. *Proc Natl Acad Sci U S A* **2015,** *112* (28), E3661-8.

75.   Anil-Inevi, M.; Yaman, S.; Yildiz, A. A.; Mese, G.; Yalcin-Ozuysal, O.; Tekin, H. C.; Ozcivici, E., Biofabrication of in situ Self Assembled 3D Cell Cultures in a Weightlessness Environment Generated using Magnetic Levitation. *Sci Rep* **2018,** *8* (1), 7239.

76.   Zhao, W.; Cheng, R.; Miller, J. R.; Mao, L., Label-Free Microfluidic Manipulation of Particles and Cells in Magnetic Liquids. *Adv Funct Mater* **2016,** *26* (22), 3916-3932.

77.   Zhu, T.; Marrero, F.; Mao, L., Continuous separation of non-magnetic particles inside ferrofluids. *Microfluidics and Nanofluidics* **2010,** *9* (4-5), 1003-1009.

78.   Zhao, W.; Zhu, T.; Cheng, R.; Liu, Y.; He, J.; Qiu, H.; Wang, L.; Nagy, T.; Querec, T. D.; Unger, E. R.; Mao, L., Label-Free and Continuous-Flow Ferrohydrodynamic Separation of HeLa Cells and Blood Cells in Biocompatible Ferrofluids. *Adv Funct Mater* **2016,** *26* (22), 3990-3998.

79.   Zhao, W.; Cheng, R.; Jenkins, B. D.; Zhu, T.; Okonkwo, N. E.; Jones, C. E.; Davis, M. B.; Kavuri, S. K.; Hao, Z.; Schroeder, C.; Mao, L., Label-free ferrohydrodynamic cell separation of circulating tumor cells. *Lab Chip* **2017,** *17* (18), 3097-3111.

80.   Zhao, W.; Liu, Y.; Jenkins, B. D.; Cheng, R.; Harris, B. N.; Zhang, W.; Xie, J.; Murrow, J. R.; Hodgson, J.; Egan, M.; Bankey, A.; Nikolinakos, P. G.; Ali, H. Y.; Meichner, K.; Newman, L. A.; Davis, M. B.; Mao, L., Tumor antigen-independent and cell size variation-inclusive enrichment of viable circulating tumor cells. *Lab Chip* **2019,** *19* (10), 1860-1876.

81.   Baday, M.; Ercal, O.; Sahan, A. Z.; Sahan, A.; Ercal, B.; Inan, H.; Demirci, U., Density Based Characterization of Mechanical Cues on Cancer Cells Using Magnetic Levitation. *Adv Healthc Mater* **2019**, e1801517.

82.   Duffy, D. C.; McDonald, J. C.; Schueller, O. J. A.; Whitesides, G. M., Rapid Prototyping of Microfluidic Systems in Poly(dimethylsiloxane). *Analytical Chemistry* **1998,** *70* (23), 4974-4984.

83.   Duffy, D. C.; Schueller, O. J.; Brittain, S. T.; Whitesides, G. M., Rapid prototyping of microfluidic switches in poly (dimethyl siloxane) and their actuation by electro-osmotic flow. *Journal of Micromechanics and Microengineering* **1999,** *9* (3), 211.

84.   Bhattacharya, S.; Datta, A.; Berg, J. M.; Gangopadhyay, S., Studies on surface wettability of poly(dimethyl) siloxane (PDMS) and glass under oxygen-plasma treatment and correlation with bond strength. *Journal of Microelectromechanical Systems* **2005,** *14* (3), 590-597.

85.   Zhou, R.; Wang, C., Multiphase ferrofluid flows for micro-particle focusing and separation. *Biomicrofluidics* **2016,** *10* (3), 034101.

86.   McDonald, J. C.; Duffy, D. C.; Anderson, J. R.; Chiu, D. T.; Wu, H.; Schueller, O. J.; Whitesides, G. M., Fabrication of microfluidic systems in poly(dimethylsiloxane). *Electrophoresis* **2000,** *21* (1), 27-40.

87.   Dang, K.; Morrison, D. W. G.; Demirci, U.; Khademhosseini, A., Plasma in Microchannel. In *Encyclopedia of Microfluidics and Nanofluidics*, Li, D., Ed. Springer US: Boston, MA, 2008; pp 1684-1691.

88.   Hillborg, H.; Gedde, U., Hydrophobicity recovery of polydimethylsiloxane after exposure to corona discharges. *Polymer* **1998,** *39* (10), 1991-1998.

89.   Xiong, L.; Chen, P.; Zhou, Q., Adhesion promotion between PDMS and glass by oxygen plasma pre-treatment. *Journal of Adhesion Science and Technology* **2014,** *28* (11), 1046-1054.

90.   Chaudhury, M. K.; Whitesides, G. M., Direct measurement of interfacial interactions between semispherical lenses and flat sheets of poly (dimethylsiloxane) and their chemical derivatives. *Langmuir* **1991,** *7* (5), 1013-1025.

91.   Gajasinghe, R. W. R. L.; Senveli, S. U.; Rawal, S.; Williams, A.; Zheng, A.; Datar, R. H.; Cote, R. J.; Tigli, O., Experimental study of PDMS bonding to various substrates for monolithic microfluidic applications. *Journal of Micromechanics and Microengineering* **2014,** *24* (7).

92.   Kirkness, M. W. H.; Korosec, C. S.; Forde, N. R., Modified Pluronic F127 Surface for Bioconjugation and Blocking Nonspecific Adsorption of Microspheres and Biomacromolecules. *Langmuir* **2018,** *34* (45), 13550-13557.

93.   Luk, V. N.; Mo, G.; Wheeler, A. R., Pluronic additives: a solution to sticky problems in digital microfluidics. *Langmuir* **2008,** *24* (12), 6382-9.

94.   Tekın, H. C. In *Determining densities of microparticles in a magnetic levitation platform using automated digital image analysis*, 2018 26th Signal Processing and Communications Applications Conference (SIU), IEEE: 2018; pp 1-4.

95.   Gwak, H.; Kim, J.; Kashefi-Kheyrabadi, L.; Kwak, B.; Hyun, K. A.; Jung, H. I., Progress in Circulating Tumor Cell Research Using Microfluidic Devices. *Micromachines (Basel)* **2018,** *9* (7).

96.   Burinaru, T. A.; Avram, M.; Avram, A.; Marculescu, C.; Tincu, B.; Tucureanu, V.; Matei, A.; Militaru, M., Detection of Circulating Tumor Cells Using Microfluidics. *ACS Comb Sci* **2018,** *20* (3), 107-126.